Supplementary Information

Enhancing Efficiency and Brightness of Deep-Blue Phosphorescent Organic Light-Emitting Diodes Through Narrowband Pt(II) Emitters

Chengyao Zhang,[1] Kewei Xu,[1] Yuankuo Liu,[1] Jianqiang Chen,[1] Yun-Fang Yang,[1] Yuanbin She,[1] Guijie Li[1]*

[1] Center for Phosphorescent Material Research, State Key Laboratory of Green Chemical Synthesis and Conversion Technology, College of Chemical Engineering, Zhejiang University of Technology, Hangzhou, Zhejiang, 310014, P. R. China

* Guijie Li. E-mail: guijieli@zjut.edu.cn

Table of Contents

Materials and Methods

Synthesis and Structural Characterization. Unless noted, all commercial reagents were purchased and used as received without further purification. ^{1}H NMR spectra were recorded at 400 or 500 MHz, and ^{13}C NMR spectra were recorded at 100 or 125 MHz NMR Bruker instruments in $CDCl_3$ or DMSO-d_6 solutions and chemical shifts were referenced to tetramethylsilane (TMS) or residual protiated solvent. If $CDCl_3$ was used as solvent, ^{1}H NMR spectra were recorded with TMS (δ = 0.00 ppm) or residual $CHCl_3$ (δ = 7.26 ppm) as internal references; ^{13}C NMR spectra were recorded with TMS (δ = 0.00 ppm) or $CDCl_3$ (δ = 77.00 ppm) as internal references. If DMSO-d_6 was used as solvent, ^{1}H NMR spectra were recorded with TMS (δ = 0.00 ppm) or residual DMSO (δ = 2.50 ppm) as internal references; ^{13}C NMR spectra were recorded with TMS (δ = 0.00 ppm) and DMSO-d_6 (δ = 39.52 ppm) as internal references. The following abbreviations (or combinations thereof) were used to explain ^{1}H NMR ultiplicities: s = singlet, d = doublet, t = triplet, q = quartet, p = quintet, m = multiplet, br = broad. All of the new compounds were analyzed for HRMS on a Waters mass spectrometer using electrospray ionization in positive ion mode of ESI-Q-TOF.

X-ray Crystallography. X-ray diffraction data were collected at 170 K on a Bruker D8 Venture diffractometer using graphite-monochromated Mo-Kα radiation (λ = 0.71073 Å) from a rotating anode generator.

Quantum Chemical Calculations. The theoretical calculations were performed using Gaussian 09 package. The molecular geometries of ground states (S_0) were optimized with the density functional theory (DFT) method at the B3LYP level. The DFT calculations were performed using a B3LYP function with a basis set of 6-31G(d) for C, H, O and N atoms; the LANL2DZ basis set with ECP was used for Pt atoms.

Electrochemistry. Cyclic voltammetry and different pulsed voltammetry were performed using a CH1760E electrochemical analyzeraccording previous report. 0.1 M tetra-*n*-butylammonium hexafluorophosphate was used as the supporting electrolyte, anhydrous *N*, *N*-dimethylformamide, was used as the solvents for the E_{ox} and E_{red} measurements, and the solutions were bubbled with nitrogen for 15 min prior to the test. Silver wire, platinum wire and glassy carbon were used as pseudoreference electrode, counter electrode, and working electrode respectively. Scan rate was 300 mV/s. The redox potentials are based on the values measured from different pulsed voltammetry and are reported relative to an internal reference ferrocenium/ferrocene (Cp_2Fe/Cp_2Fe^+). The reversibility of reduction or oxidation was determined using CV. As defined, if the magnitudes of the peak anodic and the peak cathodic current have an equal magnitude as scan speeds of 100 mV/s or slower, then the process is considered reversible; if the magnitudes of the peak anodic and the peak cathodic currents are not equal, but the return sweeps are nonzero, the process is considered quasi-reversible; otherwise, the process is considered irreversible.

Photophysical Measurements. The absorption spectra were measured on a Hitachi U-3900 UV−VS

Spectrometer. Steady state emission experiments were performed on HITACHI F-7000 spectrometer. Low temperature (77 K) emission spectra and lifetimes were measured in 2-MeTHF cooled with liquid nitrogen. Lifetime measurements and quantum efficiency were measured using an Edinburgh FS5 Spectrofluorometer equipped with an integrating sphere.

OLED Fabrication and Characterization. OLEDs were fabricated and tested in LN-FS1122 Evaporation System (Shenyang Yarunfeng Technology Co., Ltd.). All devices were fabricated by vacuum thermal evaporation, and were tested outside glove box after encapsulation. Prior to deposition, the prepatterned indium-tin-oxide (ITO) coated glass substrates were cleaned by subsequent sonication in deionized water, acetone, and isopropanol. The metal layer and organic layers were fabricated by vacuum thermal evaporation on the cleaned ITO glass substrate under vacuum (< 4×10^{-4} Pa) with 4 Å/s deposition rate for aluminum cathode and 2 Å/s for organic layers. OLEDs were fabricated using a device structure of indium tin oxide (ITO)/2,3,6,7,10,11-hexacyano-1,4,5,8,9,12-hexaazatriphenylene (HATCN) (20 nm)/1,1'-bis[4-(di-*p*-tolylamino)phenyl]cyclohexane (TAPC, 60 nm)/9-(3-(triphenylsilyl)phenyl)-9*H*-3,9′-bicarbazole (SiCzCz, 5 nm)/8 wt.% emitter:65 wt.% SiCzCz:27 wt.% 9,9′-(6-(3-(triphenylsilyl)phenyl)-1,3,5-triazine-2,4-diyl)bis(9*H*-carbazole) (SiTrzCz2) (35 nm)/2-phenyl-4,6-bis(3-(triphenylsilyl)phenyl)-1,3,5-triazine (mSiTrz, 5 nm)/mSiTrz:lithium quinolin-8-olate (Liq) (50:50, 31 nm)/LiF (1.5 nm)/Al. The device areas were 9.00 mm^2 (3.0 mm × 3.0 mm). The current density-voltage-luminance characteristics of OLEDs were measured using a Keithey 2400 Source meter and a Keithey 2000 Source multimeter equipped with a calibrated silicon photodiode following standard procedures [Forrest, S. R., Bradley, D. D. C. & Thompson, M. E. Measuring the efficiency of organic light-emitting devices. *Adv. Mater.* **15**, 1043–1048 (2003)]. The electroluminescence (EL) spectra were recorded with a multichannel spectrometer (PMA12, Hamamatsu Photonics).

Synthesis and Characterization of Tetradentate Pt(II) Complexes

Synthesis of **PtODP**:

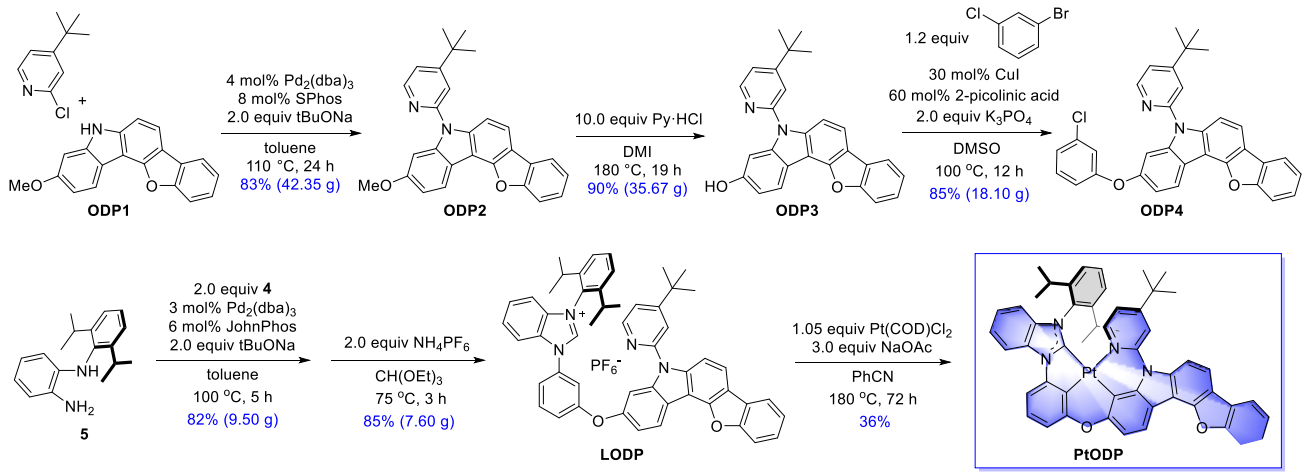

Synthesis of 5-(4-(*tert*-butyl)pyridin-2-yl)-5*H*-benzofuro[3,2-*c*]carbazol-3-ol (**ODP2**): 3-Methoxy-5*H*-benzofuro[3,2-*c*]carbazole **ODP1** (34.86 g, 121.33 mmol, 1.0 equiv), 4-(*tert*-butyl)-2-chloropyridine (24.70 g, 145.59 mmol, 1.2 equiv), *t*-BuONa (23.32 g, 242.66 mmol, 2.0 equiv), $Pd_2(dba)_3$ (4.44 g, 4.85 mmol, 4 mol%) and dicyclohexyl(2',6'-dimethoxybiphenyl-2-yl)phosphane (SPhos, 3.98 g, 9.71 mmol, 8 mol%) were added sequentially to a dry three-necked flask equipped with a magnetic stir bar. The flask was evacuated and backfilled with nitrogen, this evacuation and backfill procedure was repeated twice. Then toluene (300 mL) was added into the flask under nitrogen atmosphere at room temperature. Then the flask was placed in an oil bath and the reaction mixture was stirred at 110 ℃ for 24 hours, the reaction was monitored by TLC until the reaction was completed. The reaction mixture was cooled down to room temperature, filtered and washed with ethyl acetate. The filtrate was concentrated under reduced pressure and the residue was purified through column chromatography on silica gel (eluent: petroleum ether/ethyl acetate = 30:1−20:1) to obtain the desired product as a brown solid 42.35 g in 83% yield. ^{1}H NMR (500 MHz, $CDCl_3$): δ (ppm) 1.43 (s, 9H), 3.90 (s, 3H), 7.06 (dd, J = 8.5, 2.0 Hz, 1H), 7.34 (d, J = 2.0 Hz, 1H), 7.36 (dd, J = 5.5, 2.0 Hz, 1H), 7.38 (td, J = 7.5, 1.5 Hz, 1H), 7.43–7.46 (m, 1H), 7.69 (d, J = 1.0 Hz, 1H), 7.72 (d, J = 8.5 Hz, 2H), 7.90 (d, J = 8.5 Hz, 1H), 7.98 –7.99(m, 1H), 8.42 (d, J = 8.5 Hz, 1H), 8.67 (dd, J = 5.5, 0.5 Hz, 1H).

Synthesis of 5-(4-(*tert*-butyl)pyridin-2-yl)-5*H*-benzofuro[3,2-*c*]carbazol-3-ol (**ODP3**): Compound **ODP2**

(41.00 g, 97.50 mmol, 1.0 equiv) and Py·HCl (112.67 g, 975.00 mmol, 10.0 equiv) were added sequentially to a dry three-necked flask equipped with a magnetic stir bar. The flask was evacuated and backfilled with nitrogen, this evacuation and backfill procedure was repeated twice. Then DMI (10 mL) was added into the flask under nitrogen atmosphere at room temperature. Then the flask was placed in an oil bath and the reaction mixture was stirred and heated at 180 ℃ for 19 hours, the reaction was monitored by TLC until the reaction was completed. The reaction mixture was cooled down to room temperature, diluted with ethyl acetate. The mixture was washed with water, the organic layer was separated, and dried over Na_2SO_4, filtered. The filtrate was concentrated under reduced pressure and beating with ethyl acetate and petroleum ether, filtered to obtain the desired product as a white solid 35.67 g in 90% yield. ^{1}H NMR (500 MHz, DMSO-d_6): δ (ppm) 1.40 (s, 9H), 6.94 (dd, J = 8.5, 2.0 Hz, 1H), 7.17 (d, J = 2.0 Hz, 1H), 7.43 (td, J = 7.5, 0.5 Hz, 1H), 7.50 (td, J = 8.5, 1.5 Hz, 1H), 7.56 (dd, J = 5.0, 1.5 Hz, 1H), 7.70 (d, J = 9.0 Hz, 1H), 7.74 (d, J = 1.5 Hz, 1H), 7.83 (d, J = 8.5 Hz, 1H), 8.05 (d, J = 8.5 Hz, 1H), 8.15 (dd, J = 7.5, 0.5 Hz, 1H), 8.20 (d, J = 8.5 Hz, 1H), 8.67 (d, J = 5.0 Hz, 1H), 9.81 (s, 1H). ^{13}C NMR (125 MHz, DMSO): δ (ppm) 30.13, 34.94, 97.07, 107.00, 108.72, 111.22, 111.63, 113.07, 116.51 (2C), 116.81, 119.62, 120.24, 122.72, 123.24, 124.44, 125.85, 139.55, 140.64, 149.38, 149.48, 150.85, 155.55, 157.13, 163.16.

Synthesis of 5-(4-(*tert*-butyl)pyridin-2-yl)-3-(3-chlorophenoxy)-5*H*-benzofuro[3,2-*c*]carbazole (**ODP4**): Compound **ODP3** (16.74 g, 41.18 mmol, 1.0 equiv), 1-bromo-3-chlorobenzene (9.46 g, 49.42 mmol, 1.2 equiv), CuI (1.57 g, 8.24 mmol, 30 mol%), 2-picolinic acid (2.03 g, 16.47 mmol, 60 mol%) , and K_3PO_4 (17.48 g, 82.36 mmol, 2.0 equiv) were added sequentially to a dry three-necked flask equipped with a magnetic stir bar. The flask was evacuated and backfilled with nitrogen, this evacuation and backfill procedure was repeated twice. Then DMSO (200 mL) was added into the flask under nitrogen atmosphere at room temperature. Then the flask was placed in an oil bath and the reaction mixture was stirred at 100 ℃ for 12 hours, the reaction was monitored by TLC until the reaction was completed. The reaction mixture was cooled down to room temperature, and diluted with ethyl acetate. The mixture was washed with water, the organic layer was separated, and dried over Na_2SO_4, filtered. The filtrate was concentrated under reduced pressure and the residue was purified through column chromatography on silica gel (eluent: petroleum ether/ethyl acetate = 30:1) to obtain the desired product as a white solid 18.10 g in 85% yield. ^{1}H NMR (500 MHz, DMSO): δ (ppm) 1.32 (s, 9H), 7.10 (ddd, J = 8.5, 2.5, 1.0 Hz, 1H), 7.17–7.27 (m, 3H), 7.33 (d, J = 2.0 Hz, 1H), 7.43 (t, J = 8.5 Hz, 1H), 7.46 (td, J = 7.5, 1.0 Hz, 1H), 7.50–7.56 (m, 2H), 7.74 (d, J = 2.0 Hz, 1H), 7.80 (d, J = 8.5 Hz, 1H), 7.88 (d, J = 8.0 Hz, 1H), 8.186 (d, J = 8.5 Hz, 1H), 8.193 (dd, J = 7.5, 2.5 Hz, 1H), 8.45 (d, J = 8.5 Hz, 1H), 8.64 (d, J = 5.5 Hz, 1H).

Synthesis of N^1-(2,6-diisopropylcyclohexa-1,3-dien-1-yl)benzene-1,2-diamine (**5**): Compound

N-(2,6-diisopropylcyclohexa-1,3-dien-1-yl)-2-nitroaniline (6.0 g, 20.11 mmol, 1.0 equiv) and $SnCl_2 \cdot 2H_2O$ (18.15 g, 80.43 mmol, 4.0 equiv) were added sequentially to a dry three-necked flask equipped with a magnetic stir bar. The flask was evacuated and backfilled with nitrogen, this evacuation and backfill procedure was repeated twice. Then EtOH (60 mL) and ethyl acetate (60 mL) were added into the flask under nitrogen atmosphere at room temperature. Then the flask was placed in an oil bath and the reaction mixture was stirred and heated at 78 ℃ for 12 hours, the reaction was monitored by TLC until the reaction was completed. The reaction mixture was cooled down to room temperature, and quenched with $NaHCO_3$. The mixture was extracted with ethyl acetate, the organic layer was separated, and dried over Na_2SO_4, filtered. The filtrate was concentrated under reduced pressure and the residue was purified through column chromatography on silica gel (eluent: petroleum ether/ dichloromethane = 15:1–10:1) to obtain the desired product as a purple solid 4.70 g in 87% yield. ^{1}H NMR (500 MHz, DMSO-d_6): δ (ppm) 1.01 (s, 6H), 1.12 (s, 6H), 3.05–3.10 (m, 2H), 4.79 (s, 2H), 5.77 (dd, *J* = 7.5, 1.0 Hz, 1H), 5.95 (s, 1H), 6.29 (td, *J* = 7.5, 1.5 Hz, 1H), 6.41 (td, *J* = 7.5, 1.5 Hz, 1H), 6.59 (dd, *J* = 7.5, 1.5 Hz, 1H), 7.18 (t, *J* = 6.0 Hz, 1H), 7.20 (s, 1H), 7.23 (dd, *J* = 9.0, 5.5 Hz, 1H).

Syntesis of 1-(3-((5-(4-(*tert*-butyl)pyridin-2-yl)-5*H*-benzofuro[3,2-*c*]carbazol-3-yl)oxy)phenyl)-3-(2,6-diisopropylphenyl)-1*H*-benzo[*d*]imidazol-3-ium(**LODP**): Compound **ODP4** (8.00 g, 15.47 mmol, 1.0 equiv), **5** (4.98 g, 18.57 mmol, 1.2 equiv), $Pd_2(dba)_3$ (425 mg, 0.46 mmol, 3 mol%), 2-(Di-tert-butylphosphino)biphenyl (JohnPhos, 277 mg, 0.93 mmol, 6 mol%), and *t*-BuONa (2.97 g, 30.95 mmol, 2.0 equiv) were added sequentially to a dry three-necked flask equipped with a magnetic stir bar. The flask was evacuated and backfilled with nitrogen, this evacuation and backfill procedure was repeated twice. Then toluene (80 mL) was added and the mixture was heated at 100 ℃ under a nitrogen atmosphere for 5 hours. After the reaction was completed, the mixture was cooled to room temperature and concentrated under reduced pressure. The residue was purified through column chromatography on silica gel (eluent: petroleum ether/ethyl acetate = 30:1) to obtain the desired product diamine as powder solid 9.50 g in 82% yield. The intermediate diamine was not stable enough and easily oxidized by air, thereby, directly used for the next step. The diamine (7.40 g, 9.88 mmol, 1.0 equiv), and NH_4PF_6 (3.22 g, 19.76 mmol, 2.0 equiv) were added to dry three-necked flask equipped with a magnetic stir bar. Then $CH(OEt)_3$ (30 mL) was added and the mixture was heated at 75 ℃ under a nitrogen atmosphere for 3 hours. After the reaction was completed by TLC monitoring, the mixture was cooled down to room temperature. Then concentrated under reduced pressure. The residue was purified through column chromatography on silica gel (eluent: petroleum ether/dichloromethane = 1:1–dichloromethane/ethyl acetate = 50:1) to obtain the desired product as powder solid 7.60 g in 85% yield. ^{1}H NMR

(500 MHz, $CDCl_3$): δ (ppm) 1.02 (d, J = 6.5 Hz, 6H), 1.23 (d, J = 7.0 Hz, 6H), 1.42 (s, 9H), 2.15–2.21 (m, 2H), 7.30 (d, J = 8.5 Hz, 1H), 7.31 (dd, J = 8.5, 1.5 Hz, 1H), 7.35 (t, J = 2.5 Hz, 1H), 7.37–7.38 (m, 1H), 7.39 (d, J = 1.5 Hz, 1H), 7.41 (s, 1H), 7.42 (s, 1H), 7.48 (td, J = 7.5, 1.0 Hz, 1H), 7.56 (dd, J = 8.0, 1.0 Hz, 1H), 7.59–7.69 (m, 6H), 7.72 (d, J = 9.0 Hz, 1H), 7.75 (t, J = 8.5 Hz, 2H), 7.95 (d, J = 8.5 Hz, 1H), 7.98 (d, J = 8.5 Hz, 1H), 8.00 (dd, J = 7.5, 0.5 Hz, 1H), 8.59 (d, J = 8.5 Hz, 1H), 8.63 (d, J = 5.5 Hz, 1H), 9.64 (s, 1H). ^{13}C NMR (125 MHz, $CDCl_3$): δ (ppm) 23.98, 24.17, 28.98, 30.52, 35.21, 103.49, 106.27, 109.17, 111.73, 113.34, 113.67, 114.29, 114.33, 116.75, 117.54, 118.00, 118.90, 119.27, 119.63, 119.88, 120.48, 122.99, 123.97, 124.82, 125.16, 125.68, 126.81, 128.75, 128.91, 129.10, 130.81, 132.11, 132.53, 132.56, 132.76, 133.04, 133.38, 140.56, 140.88, 146.14, 149.66, 150.79, 151.26, 154.05, 156.36, 159.99, 163.71. HRMS (ESI): calcd for $C_{52}H_{47}N_4O_2^+$ $[M+H]^+$ 759.3694, found 759.3669.

Synthesis of platinum(II) (**PtODP**): Ligand **LODP** (21.00 g, 23.21 mmol, 1.00 equiv), $Pt(COD)Cl_2$ (9.12 g, 24.37 mmol, 1.05 equiv), and NaOAc (5.71 g, 69.62 mmol, 3.00 equiv) were added sequentially to a dry three-necked flask equipped with a magnetic stir bar. The flask was evacuated and backfilled with nitrogen, this evacuation and backfill procedure was repeated twice. Then Benzonitrile (PhCN, 765 mL) was added and the mixture was stirred at 180 ℃ for 72 hours under a nitrogen atmosphere. After the reaction was completed, the mixture was cooled down to room temperature and extracted with dichloromethane three times, dried over Na_2SO_4, filtered, and the filtrate was concentrated under reduced pressure. The residue was purified through column chromatography on silica gel (eluent: petroleum ether/dichloromethane = 4:1–2:1) to obtain the desired product as yellow solid 7.95 g in 36% yield. ^{1}H NMR (500 MHz, $CDCl_3$): δ (ppm) 0.68–1.09 (br, 6H), 1.04–1.27 (br, 6H), 1.28 (s, 9H), 2.81–3.40 (br, 2H), 6.10 (dd, J = 6.5, 2.0 Hz, 1H), 6.96 (d, J = 8.0 Hz, 1H), 7.22 (dd, J = 8.0 , 0.5 Hz, 1H), 7.26 (d, J = 3.5 Hz, 2H), 7.28 (d, J = 8.0 Hz, 1H), 7.36–7.40 (m, 2H), 7.40–7.45 (m, 2H), 7.46–7.49 (m, 1H), 7.54 (d, J = 8.5 Hz, 1H), 7.66 (d, J = 7.5 Hz, 1H), 7.74 (d, J = 8.0 Hz, 1H), 7.77 (d, J = 8.5 Hz, 1H), 7.92 (d, J = 8.5 Hz, 1H), 8.00 (dd, J = 7.0, 0.5 Hz, 1H), 8.05 (d, J = 1.5 Hz, 1H), 8.19 (d, J = 8.0 Hz, 1H), 8.23 (d, J = 8.0 Hz, 1H), 8.66 (d, J = 6.5 Hz, 1H). HRMS (ESI): calcd for $C_{52}H_{45}N_4O_2Pt$ $[M+H]^+$ 952.3185, found 952.3185. ^{13}C NMR spectrum was not available because of the poor solubility of **PtODP** in solvents.

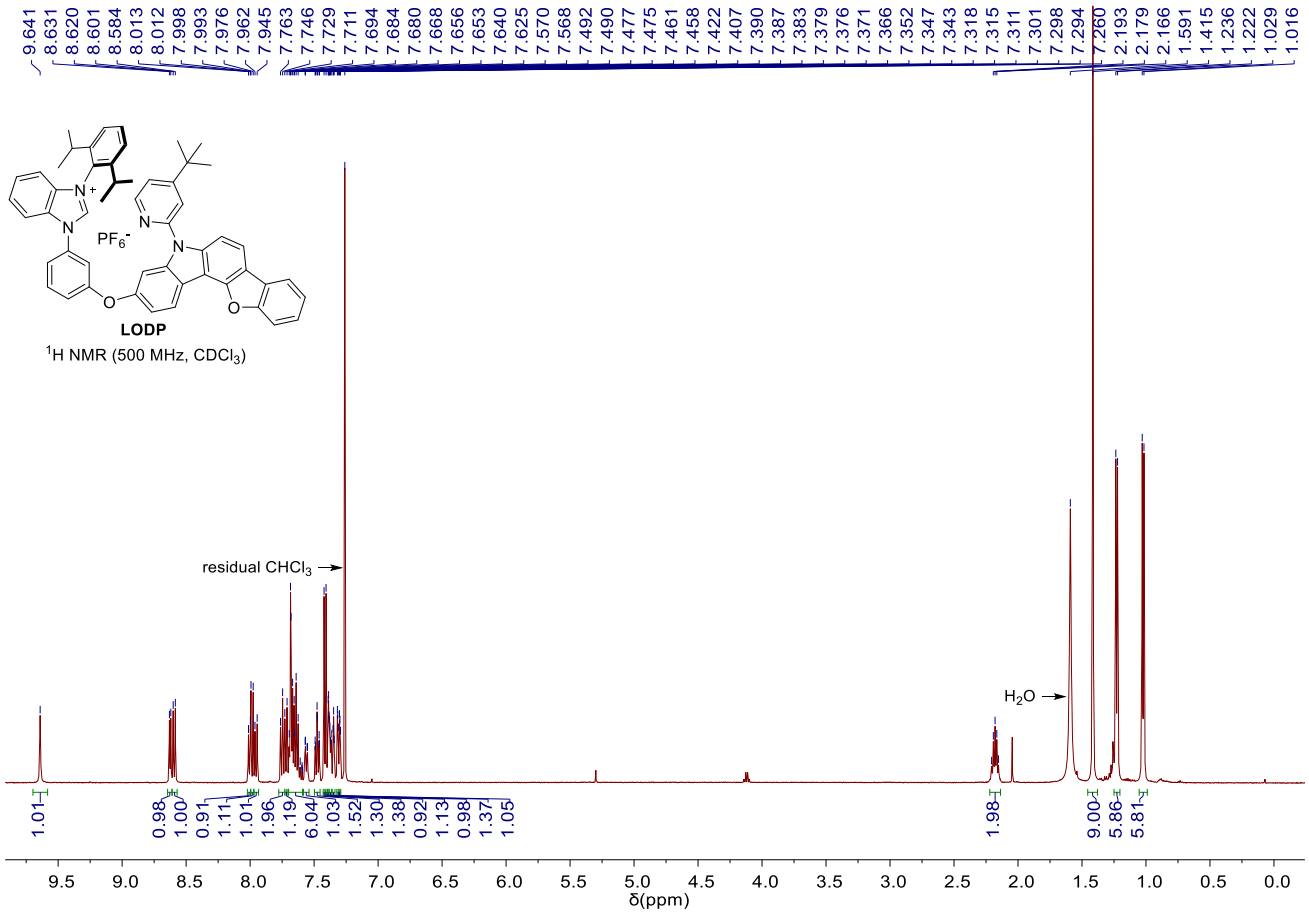
LODP
1H NMR (500 MHz, CDCl3)
residual CHCl3
H2O
δ(ppm)

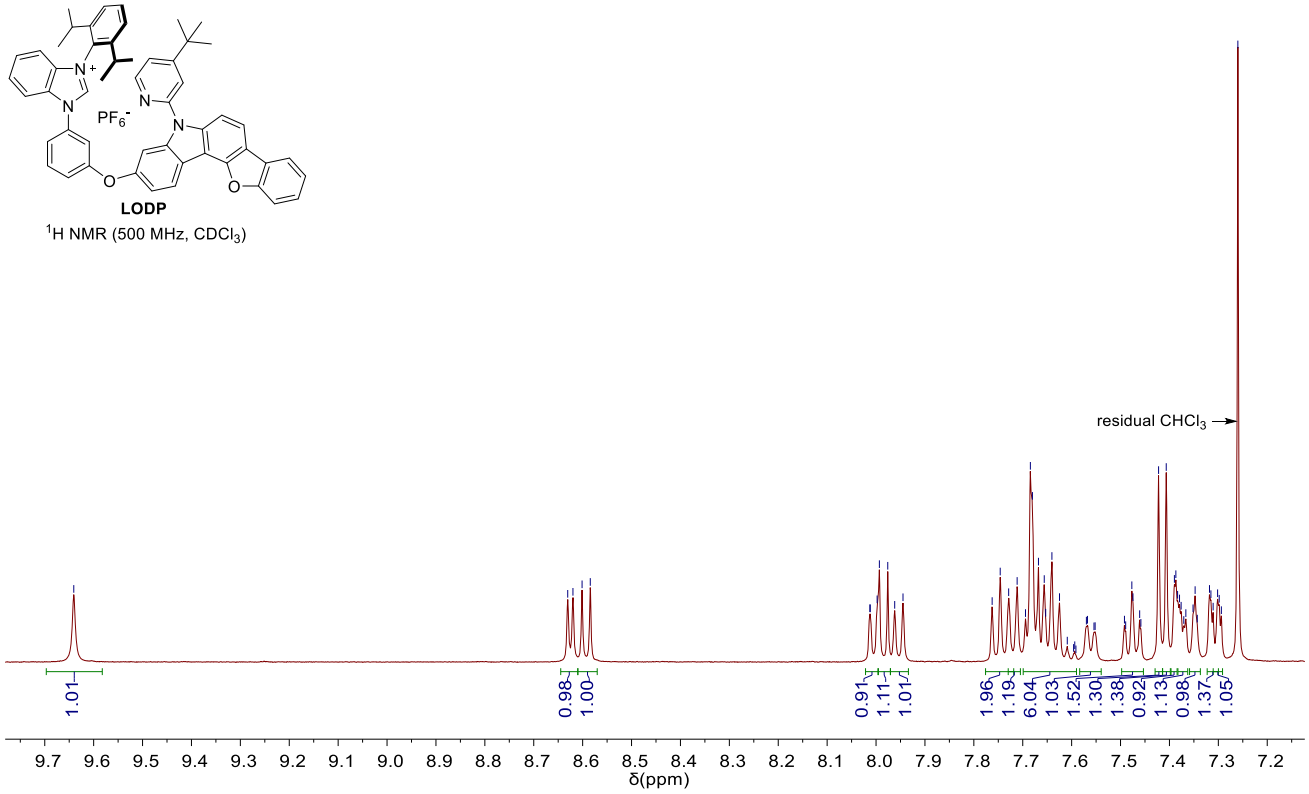
LODP
1H NMR (500 MHz, CDCl3)
residual CHCl3
δ(ppm)

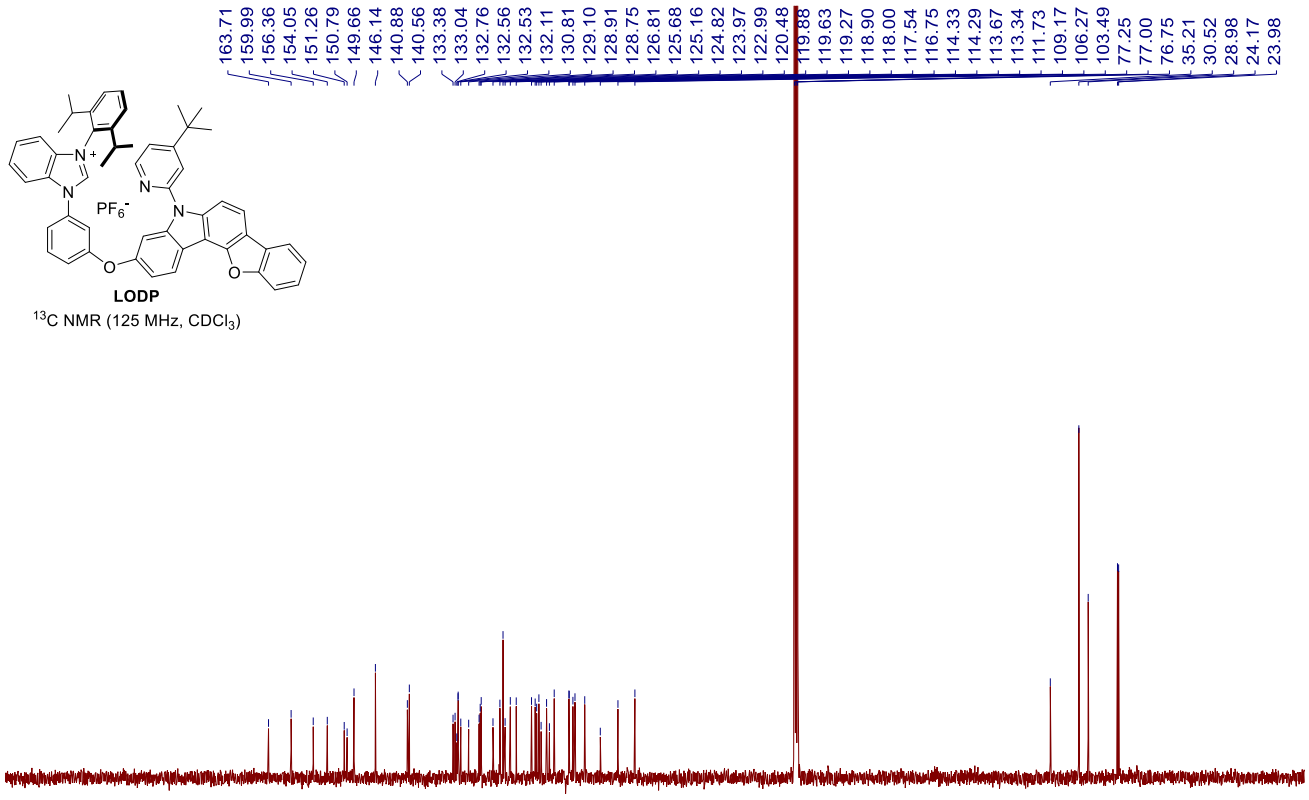
163.71
159.99
156.36
154.05
151.26
150.79
149.66
146.14
140.88
140.56
133.38
133.04
132.76
132.56
132.53
132.11
130.81
129.10
128.91
128.75
126.81
125.68
125.16
124.82
123.97
122.99
120.48
119.88
119.63
119.27
118.90
118.00
117.54
116.75
114.33
114.29
113.67
113.34
111.73
109.17
106.27
103.49
77.25
77.00
76.75
35.21
30.52
28.98
24.17
23.98
PF6-
LODP
13C NMR (125 MHz, CDCl3)
200 190 180 170 160 150 140 130 120 110 100 90 80 70 60 50 40 30 20 10 0
δ(ppm)

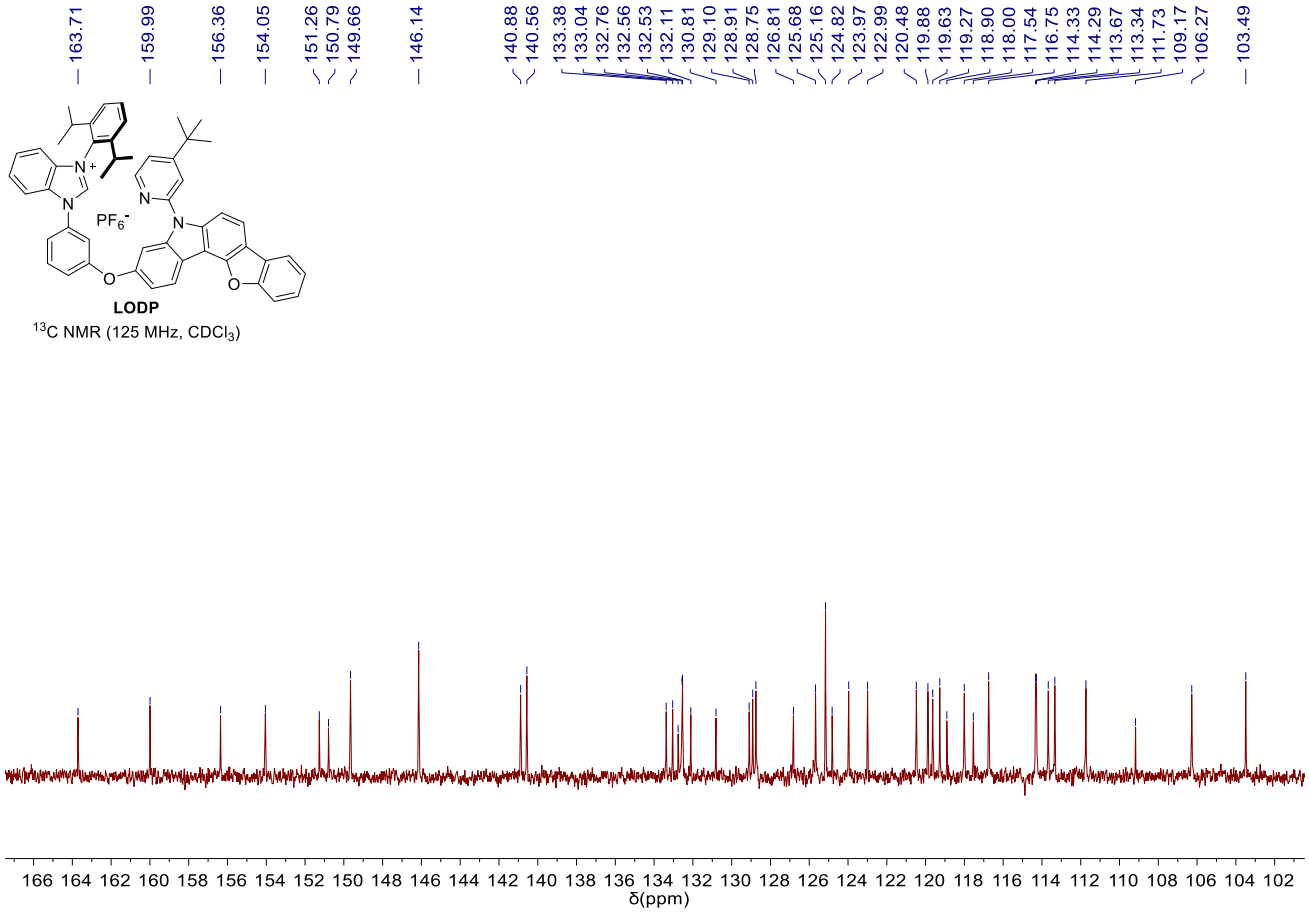
163.71
159.99
156.36
154.05
151.26
150.79
149.66
146.14
140.88
140.56
133.38
133.04
132.76
132.56
132.53
132.11
130.81
129.10
128.91
128.75
126.81
125.68
125.16
124.82
123.97
122.99
120.48
119.88
119.63
119.27
118.90
118.00
117.54
116.75
114.33
114.29
113.67
113.34
111.73
109.17
106.27
103.49
PF6-
LODP
13C NMR (125 MHz, CDCl3)
166 164 162 160 158 156 154 152 150 148 146 144 142 140 138 136 134 132 130 128 126 124 122 120 118 116 114 112 110 108 106 104 102
δ(ppm)

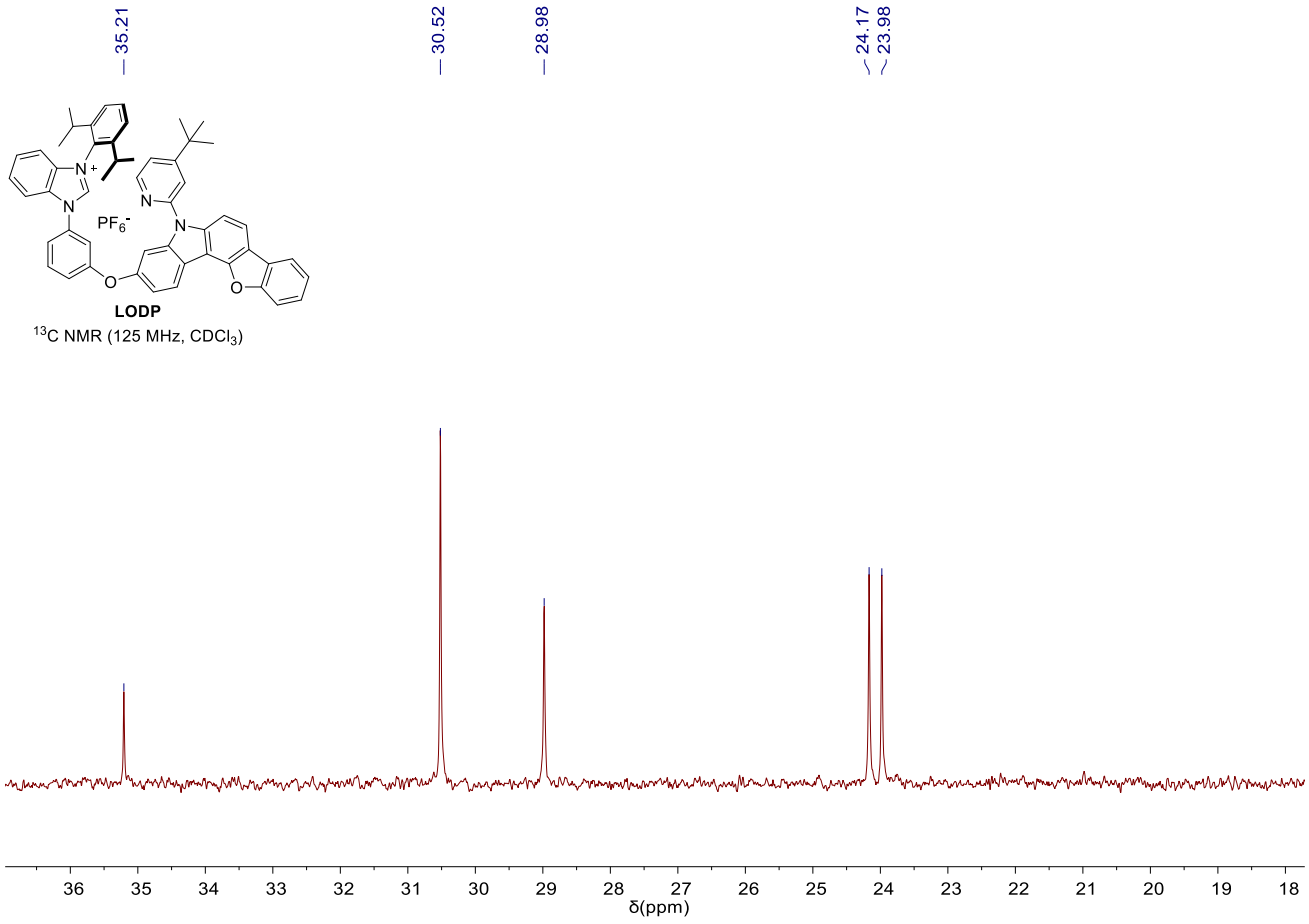
35.21
30.52
28.98
24.17
23.98
PF6-
LODP
13C NMR (125 MHz, CDCl3)
δ(ppm)

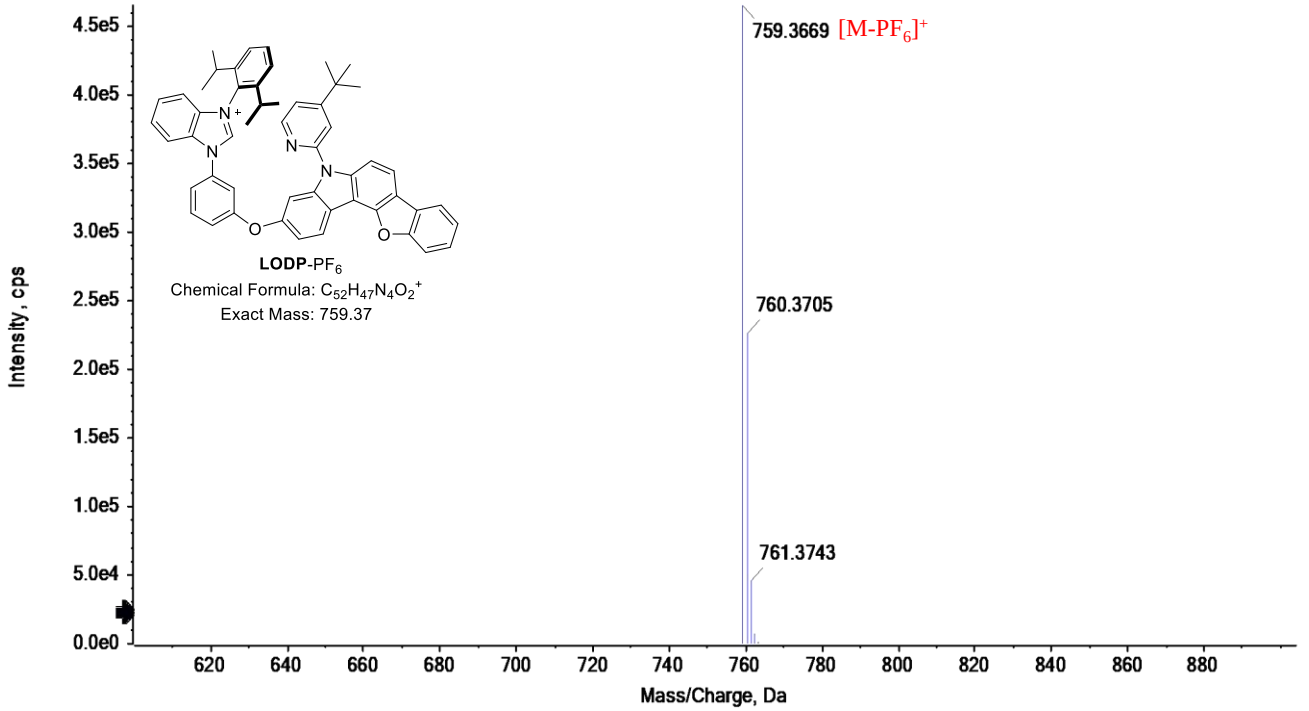
759.3669 [M-PF6]+
760.3705
761.3743
LODP-PF6
Chemical Formula: C52H47N4O2+
Exact Mass: 759.37
Intensity, cps
Mass/Charge, Da

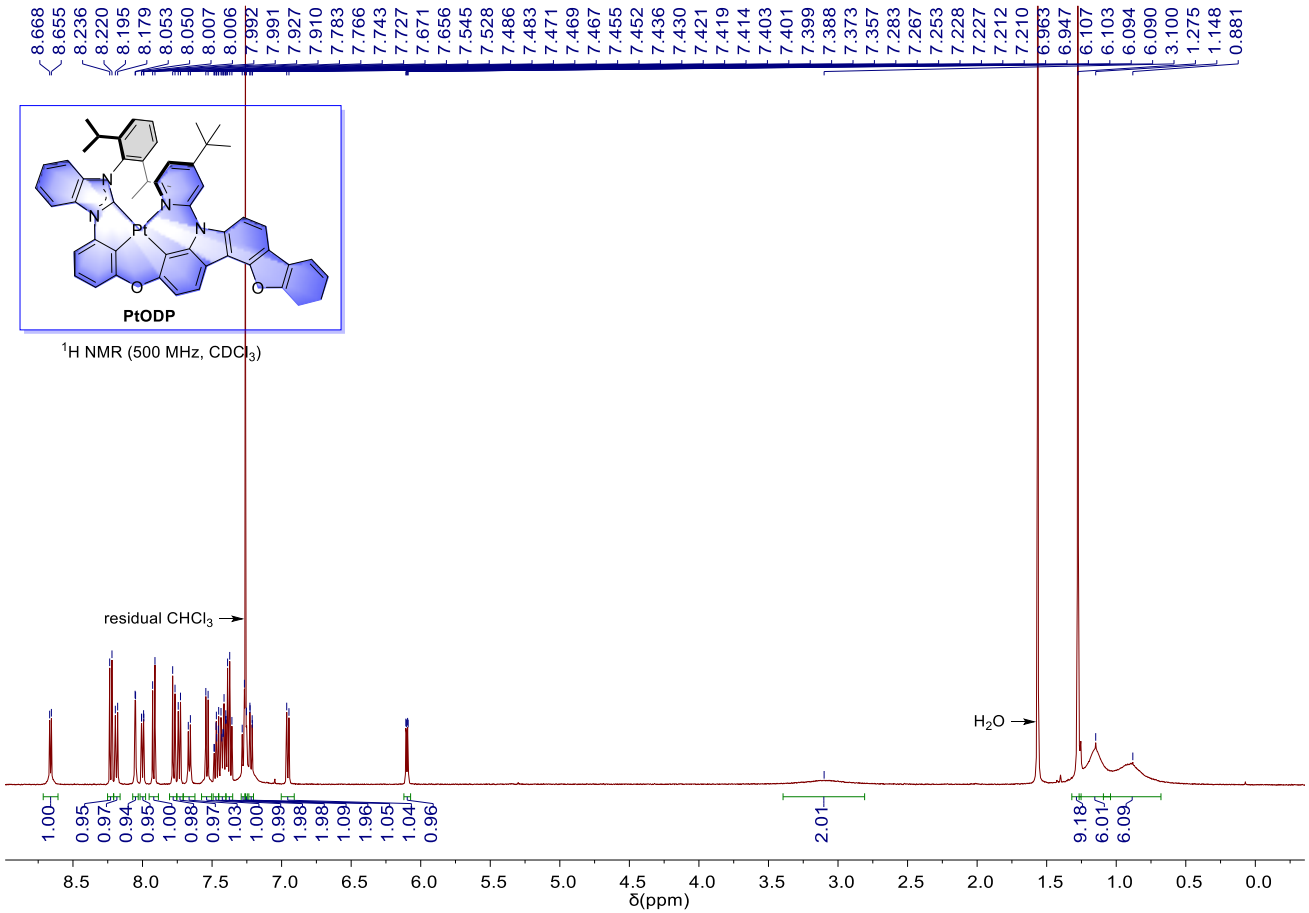
PtODP
^{1}H NMR (500 MHz, $CDCl_3$)
residual $CHCl_3$
H_2O
δ(ppm)

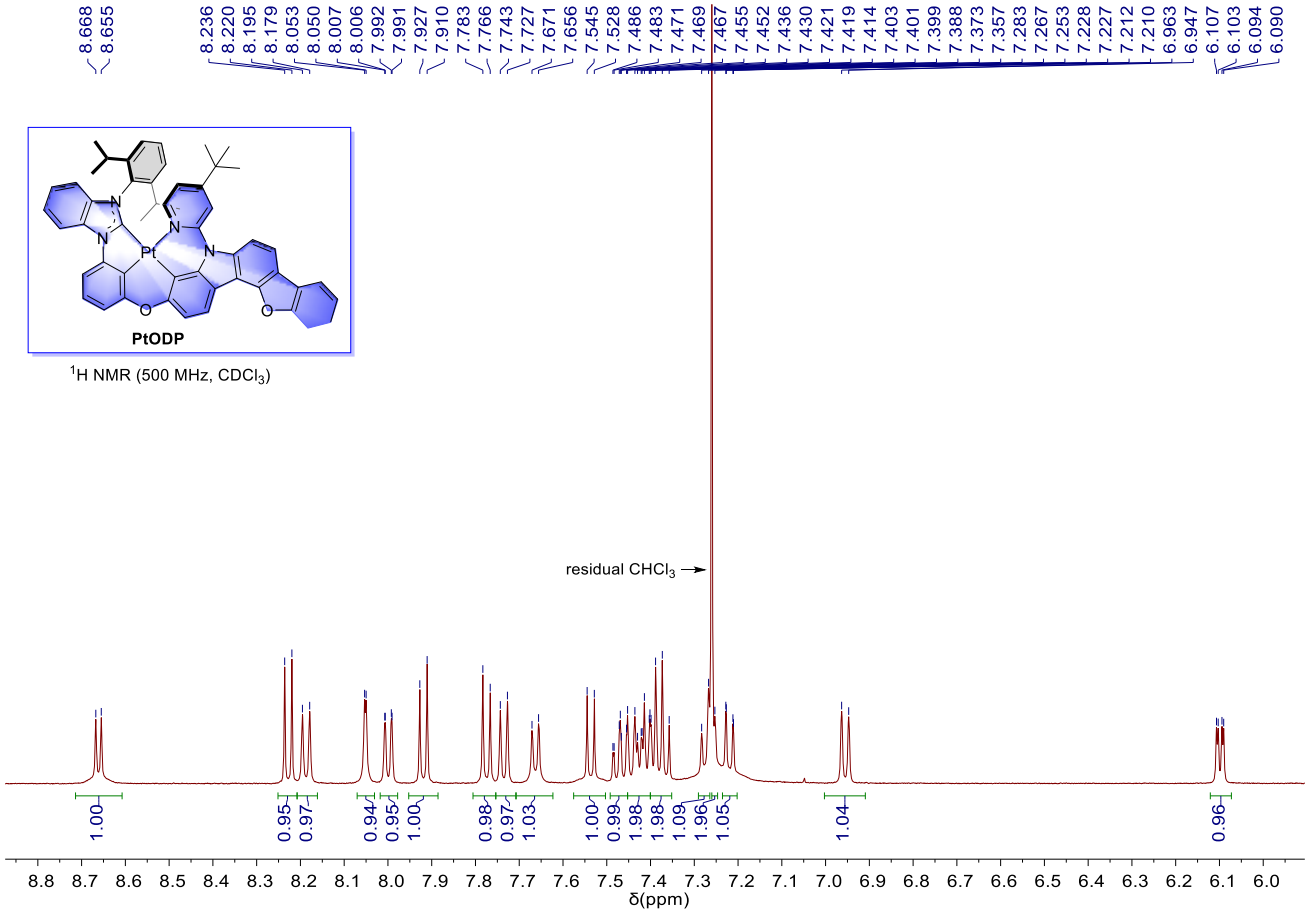
PtODP
^{1}H NMR (500 MHz, $CDCl_3$)
residual $CHCl_3$
δ(ppm)

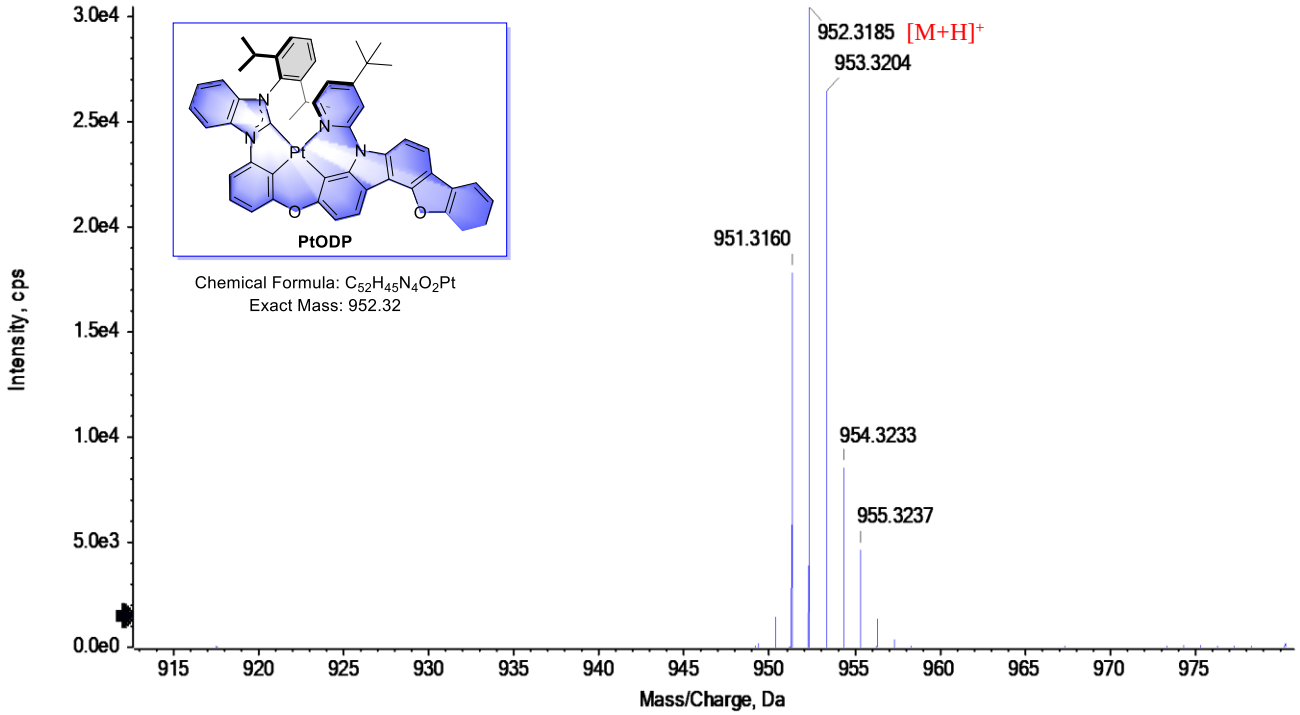
PtODP
Chemical Formula: $C_{52}H_{45}N_4O_2Pt$
Exact Mass: 952.32
952.3185 [M+H]+
953.3204
951.3160
954.3233
955.3237
Intensity, cps
Mass/Charge, Da

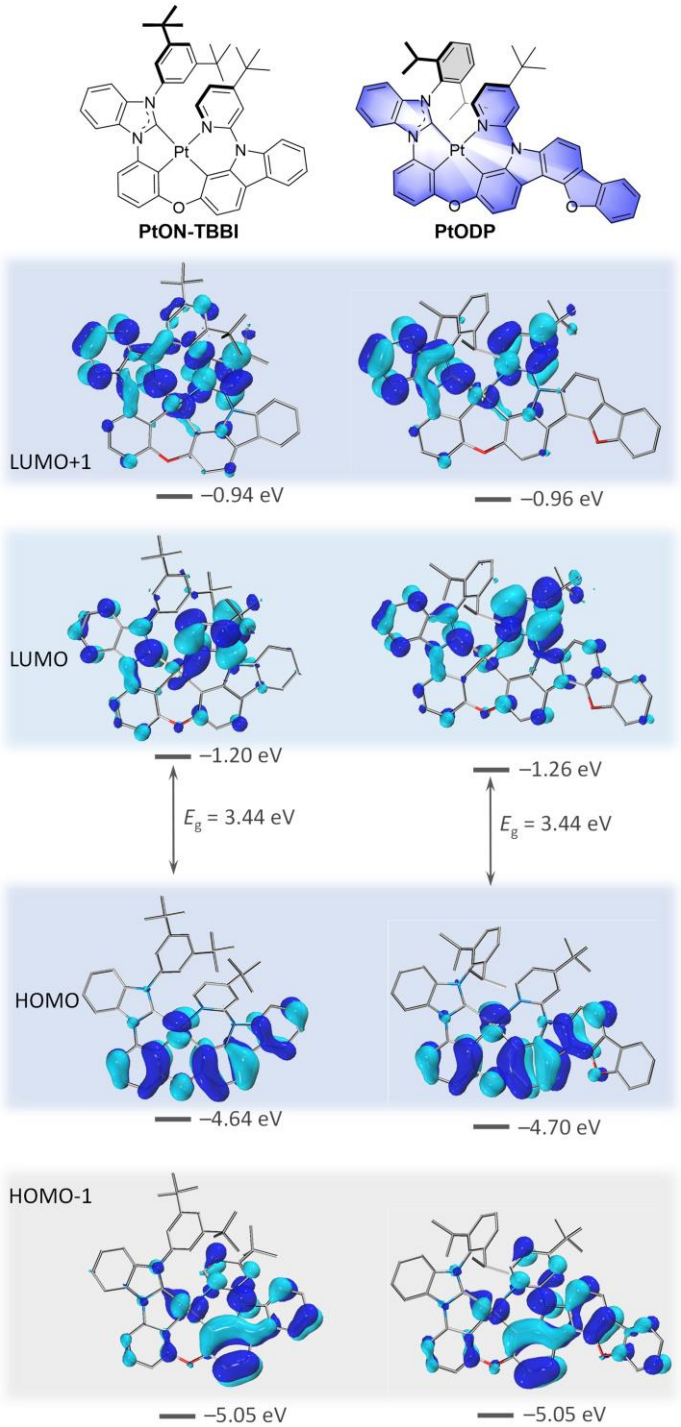

Fig. S1. Density functional theory (DFT) calculated frontier orbits of Pt(II) complexes. Frontier orbits and energy levels of PtON-TBBI and PtODP. Optimized S_0 were calculated using a B3LYP method with a basic set of 6-31G* for C, H, O, and N atoms and a LANL2DZ basic set for Pt atom.

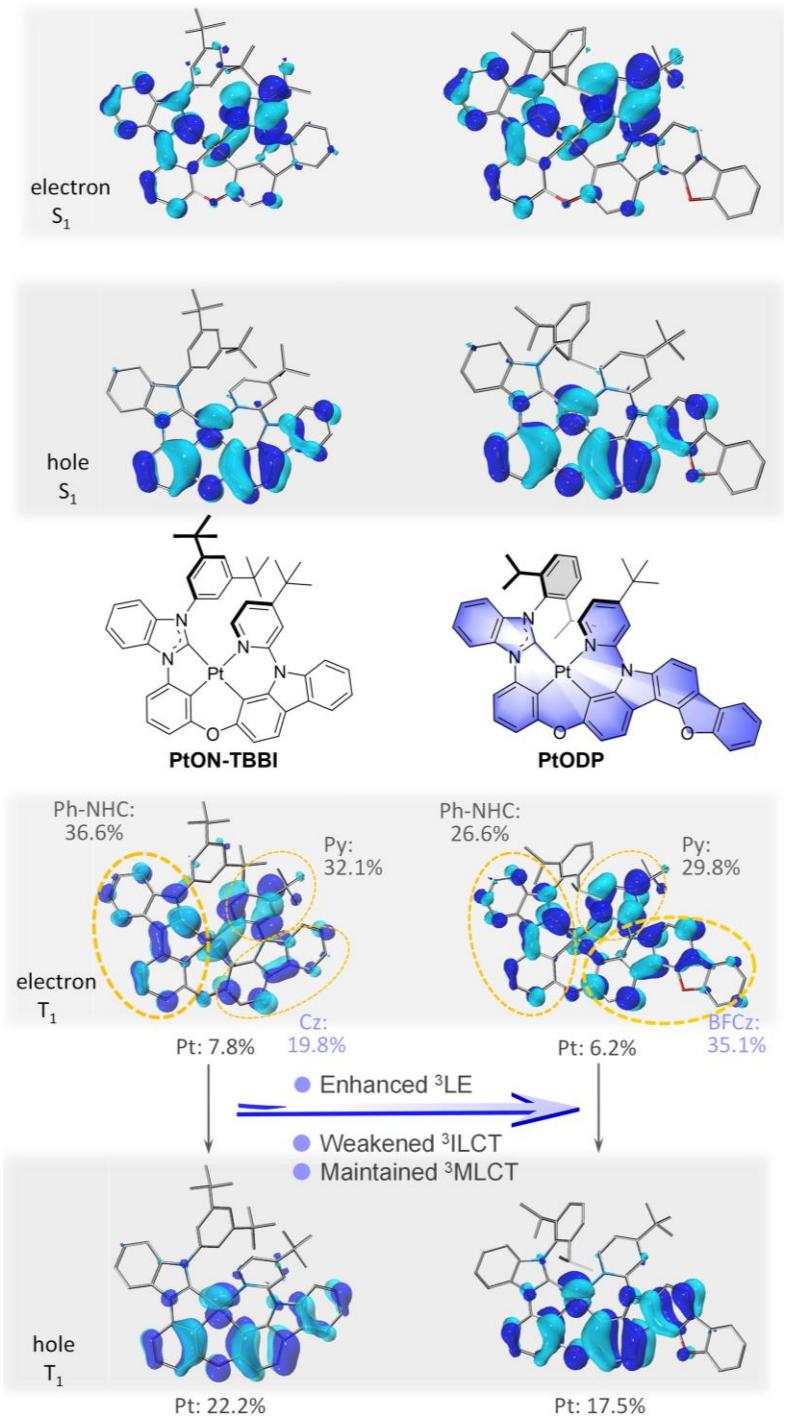

Fig. S2. Time-dependent density functional theory (TD-DFT) calculations of Pt(II) complexes. Natural transition orbital (NTO) analyses of PtON-TBBI and PtODP. Optimized S_0 were calculated using a B3LYP method with a basic set of 6-31G* for C, H, O, and N atoms and a LANL2DZ basic set for Pt atom.

Table S1. Calculated excitation energy (*E*), wavelength (λ), oscillator strength (*f*), main orbital contribution and charge characters of the excited states of PtODP[a]

excited state	energy [eV]	wavelength [nm]	*f*	major contributions
S_1	2.8303	438.06	0.0421	HOMO → LUMO (94%)
S_2	3.0767	402.98	0.0049	HOMO-2 → LUMO+1 (3%) HOMO-1 → LUMO (12%) HOMO → LUMO+1 (79%)
T_1	2.5771	481.09	0.0000	HOMO-1 → LUMO (3%) HOMO → LUMO (76%) HOMO → LUMO+2 (5%) HOMO → LUMO+6 (2%)
T_2	2.8477	435.38	0.0000	HOMO-2 → LUMO (14%) HOMO-1 → LUMO (11%) HOMO-1 → LUMO+2 (6%) HOMO → LUMO (7%) HOMO → LUMO+1 (9%) HOMO → LUMO+2 (22%)
T_3	2.9454	420.95	0.0000	HOMO-1 → LUMO (59%) HOMO → LUMO+1 (9%) HOMO → LUMO+2 (14%)
T_4	2.9768	416.50	0.0000	HOMO-2 → LUMO+1 (4%) HOMO-1→ LUMO (17%) HOMO → LUMO (7%) HOMO → LUMO+1 (58%)
T_5	3.0743	403.29	0.0000	HOMO-2 → LUMO (24%) HOMO-2 → LUMO+1 (12%) HOMO-2 → LUMO+6 (3%) HOMO-1 → LUMO+1 (7%) HOMO-1 → LUMO+2 (10%)
T_6	3.2040	386.97	0.0000	HOMO-4 → LUMO (7%) HOMO-4 → LUMO+1 (2%) HOMO-4 → LUMO+2 (4%) HOMO-2 → LUMO (6%) HOMO-2 → LUMO+1 (3%) HOMO-1 → LUMO (3%) HOMO-1 → LUMO+1 (20%) HOMO-1 → LUMO+2 (19%) HOMO → LUMO (2%) HOMO → LUMO+1 (3%) HOMO → LUMO+2 (6%) HOMO → LUMO+7 (2%)
T_7	3.2663	379.59	0.0000	HOMO-4 → LUMO+1 (2%) HOMO-4 → LUMO+2 (3%) HOMO-1 → LUMO+1 (35%) HOMO-1 → LUMO+2 (27%) HOMO → LUMO+2 (14%)

[a] Optimized S_0 were calculated using a B3LYP method with a basic set of 6-31G* for C, H, O, and N atoms and a LANL2DZ basic set for Pt atom.

Table S2. Crystal data and structure refinements of PtODP ·CH_2Cl_2

Compound	**PtODP ·CH_2Cl_2**
CCDC number	2416736
Empirical formula	$C_{53}H_{46}Cl_2N_4O_2Pt$
Formula weight	1036.93
Temperature/K	170.00
Crystal system	monoclinic
Space group	$P2_1/c$
a/Å	12.8455(4)
b/Å	14.3225(5)
c/Å	24.2024(8)
α/°	90
β/°	102.9920(10)
γ/°	90
Volume/$Å^3$	4338.8(2)
Z	4
$\rho_{calc}g/cm^3$	1.587
μ/mm^{-1}	5.155
F(000)	2080.0
Crystal size/mm^3	0.09 × 0.04 × 0.03
Radiation	GaKα (λ = 1.34139)
2Θ range for data collection/°	6.282 to 121.316
Index ranges	$-16 \leq h \leq 16$, $-18 \leq k \leq 18$, $-31 \leq l \leq 28$
Reflections collected	48646
Independent reflections	9945 [R_{int} = 0.0686, R_{sigma} = 0.0638]
Data/restraints/parameters	9945/0/566
Goodness-of-fit on F^2	1.136
Final R indexes [I>=2σ (I)]	R_1 = 0.0471, wR_2 = 0.1119
Final R indexes [all data]	R_1 = 0.0576, wR_2 = 0.1160
Largest diff. peak/hole / e $Å^{-3}$	1.36/–1.86

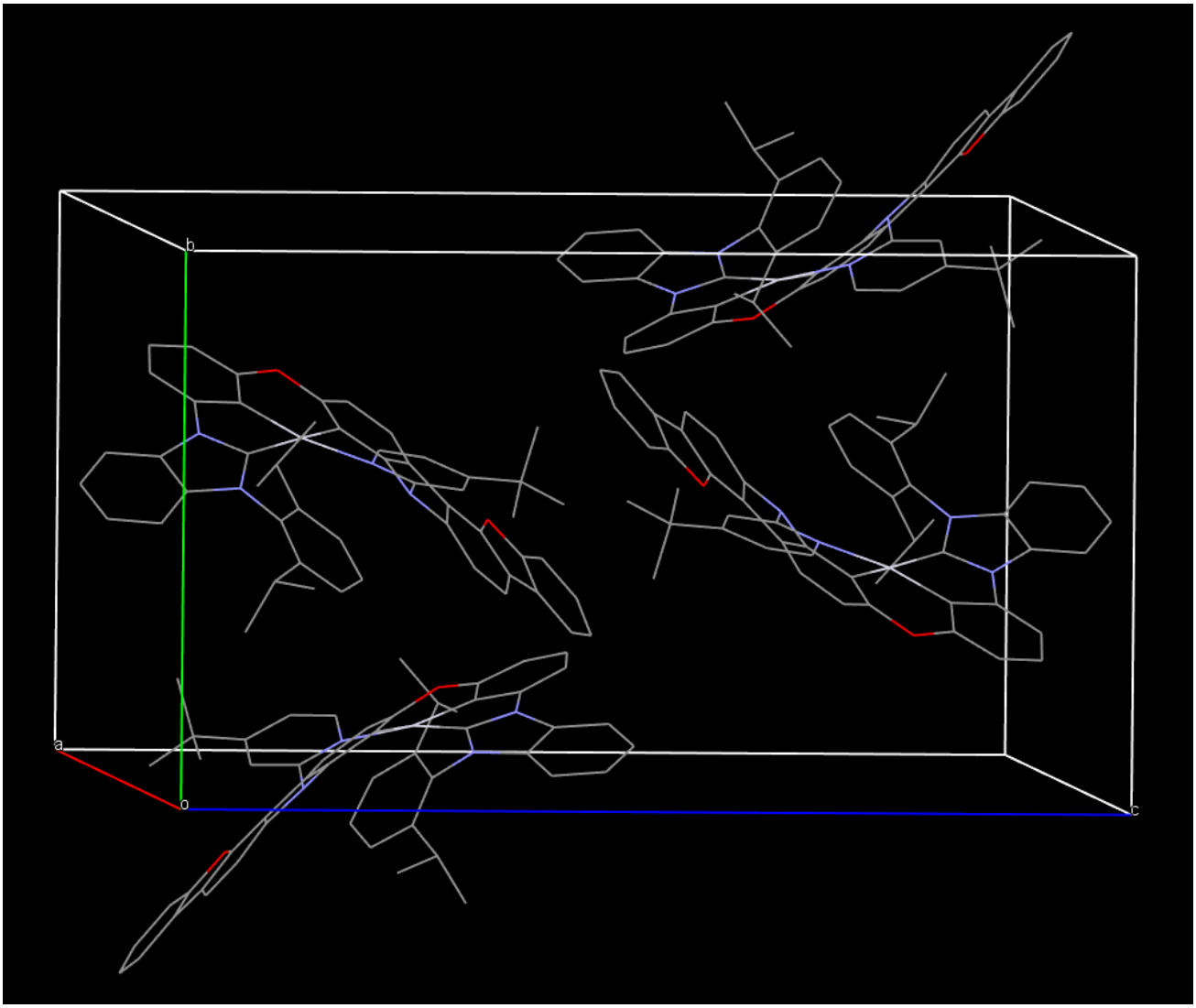

Fig. S3. The molecular packing structure of PtODP. Solvent molecules and hydrogen atoms were omitted for clarity.

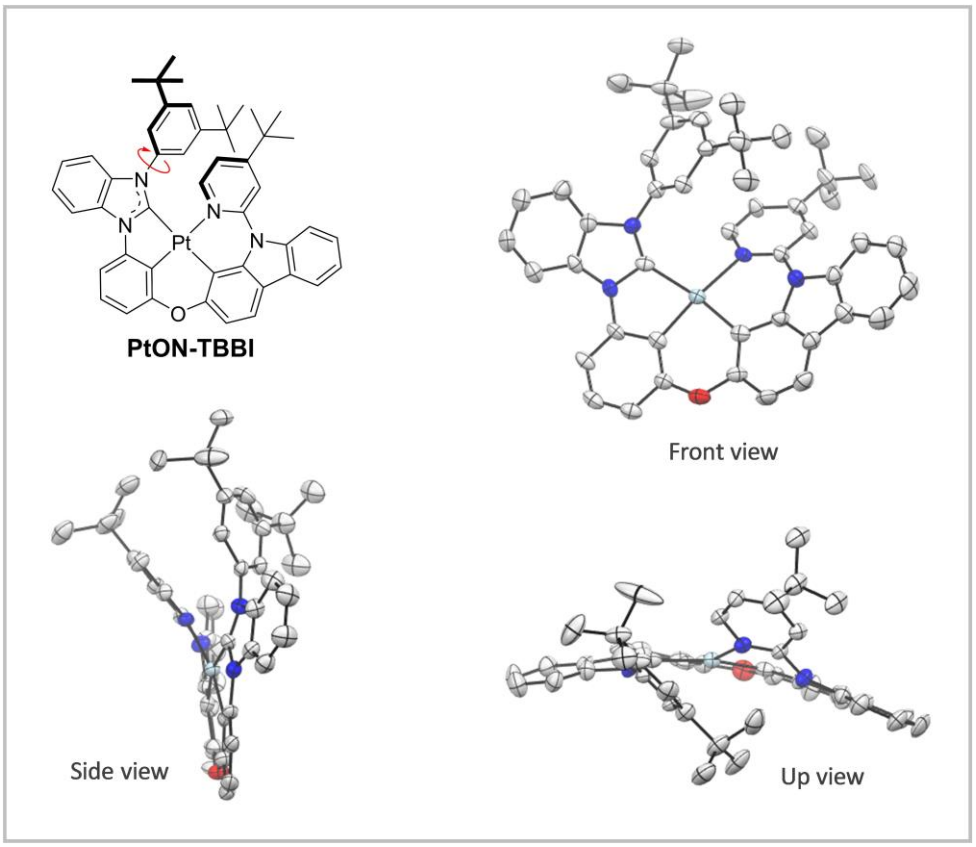

Fig. S4. ORTEP drawings of single-crystal X-ray diffraction molecular structure of PtON-TBBI (CCDC 2432339); hydrogen atoms are omitted for clarity.

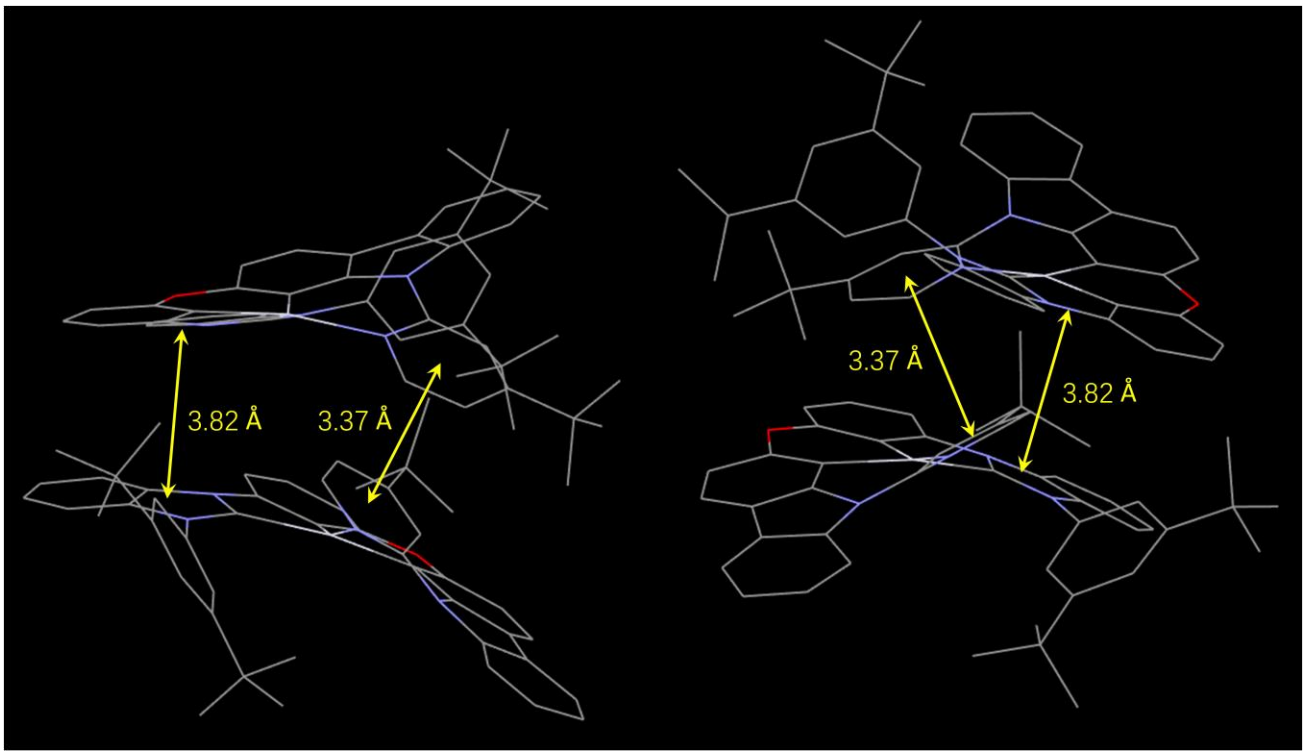

Fig. S5. The molecular packing structure of PtON-TBBI (CCDC 2432339). Hydrogen atoms were omitted for clarity.

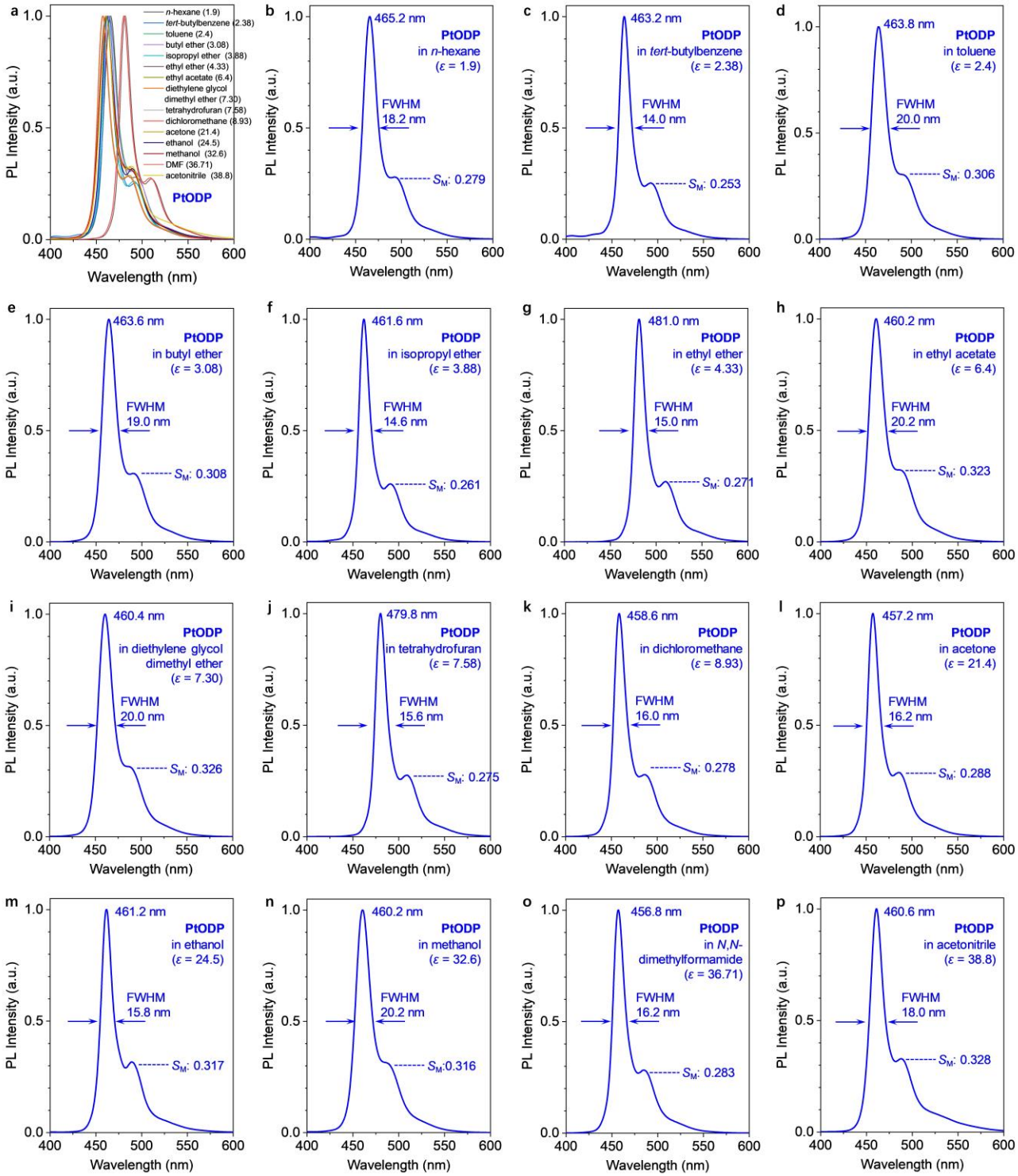

Fig. S6. Photophysical properties of PtODP in various solvents. a Photoluminescence (PL) spectra of PtODP in various solvents at room temperature. **b**–**p** PL spectra of PtODP in *n*-hexane, *tert*-butylbenzene, toluene, butyl ether, isopropyl ether, ethyl ether, ethyl acetate, diethylene glycol dimethyl ether, tetrahydrofuran, dichloromethane, acetone, ethanol, methanol, *N*,*N*-dimethylformamide (DMF), and acetonitrile at room temperature, respectively; the maximum wavelength, full-width at half-maximum (FWHM) value, and Huang–Rhys factor (S_M) value of PtODP were provided; the dielectric constant (ε) values are obtained from http://www.stenutz.eu/chem/solv23.php.

Table S3. Photophysical properties of PtODP in various solvents.

solvent	ε	λ_{max} [nm/cm^{-1}]	$\lambda_{0\text{-}1}$ [nm/cm^{-1}]	ΔE [cm^{-1}]	FWHM [nm]	S_M
n-hexane	1.90	465.2/21496	486.4/20559	937	18.2	0.279
tert-butylbenzene	2.38	463.2/21589	493.0/20284	1305	14.0	0.253
toluene	2.40	463.8/21561	488.0/20492	1069	20.0	0.306
butyl ether	3.08	463.6/21570	484.4/20644	926	19.0	0.308
isopropyl ether	3.88	461.6/21664	479.4/20859	805	14.6	0.261
ethyl ether	4.33	481.0/20790	509.5/19627	1163	15.0	0.271
ethyl acetate	6.40	460.2/21730	485.5/20597	1133	20.2	0.323
diethylene glycol dimethyl ether	7.30	460.4/21720	480.4/20816	904	20.0	0.326
tetrahydrofuran (THF)	7.58	479.8/20842	508.4/19670	1172	15.6	0.275
dichloromethane (DCM)	8.93	458.6/21805	485.8/20585	1220	16.0	0.278
acetone	21.4	457.2/21872	486.2/20568	1304	16.2	0.288
ethanol	24.5	461.2/21683	489.4/20433	1250	15.8	0.317
methanol	32.6	460.2/21730	484.8/20627	1103	20.2	0.316
N,*N*-dimethylformamide (DMF)	36.7	456.8/21891	484.6/20636	1255	16.2	0.283
acetonitrile	38.8	460.6/21711	488.2/20483	1228	18.0	0.328

ε, dielectric constant; λ_{max}, maximum wavelength; FWHM, full-width at half-maximum; S_M, Huang–Rhys factor. ΔE is the vibrational energy between λ_{max} and $\lambda_{0\text{-}1}$, $\Delta E = \lambda_{max} - \lambda_{0\text{-}1}$.

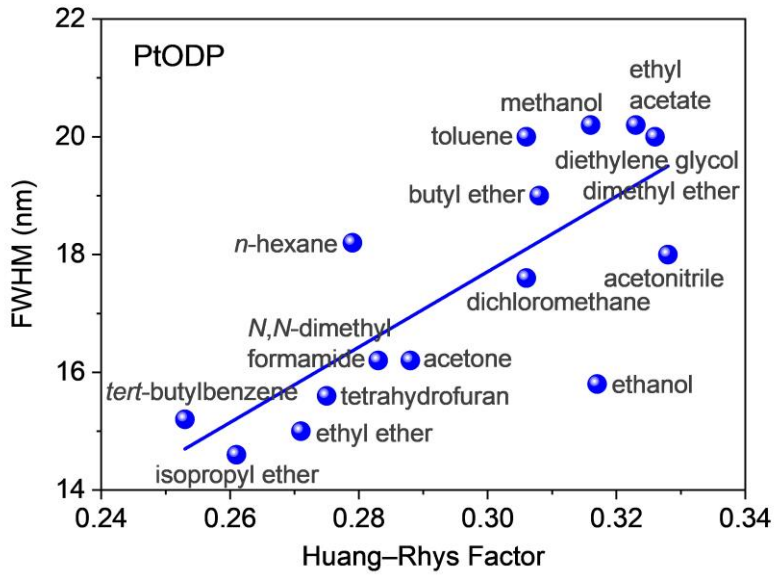

Fig. S7. Photophysical properties of PtODP. Relationship between FWHM and S_M of PtODP in various solvents.

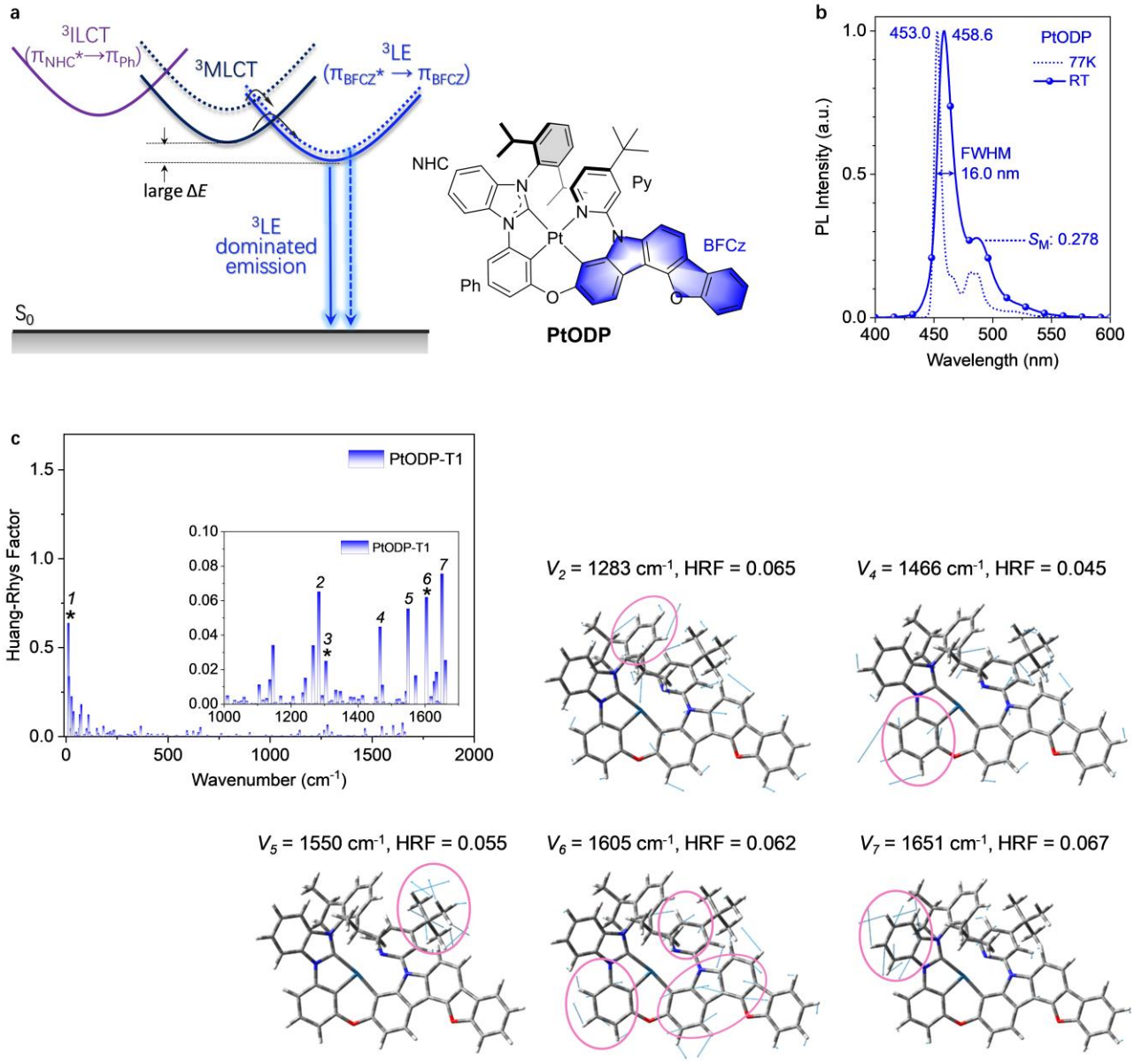

Fig. S8. Luminescence mechanism, photophysical properties and theoretical calculation of PtODP. a Potential energy surface diagram of PtODP. **b** Photoluminescence (PL) spectra of PtODP in 2-MeTHF at 77 K and in dichloromethane at room temperature. **c** Theoretically calculated Huang-Rhys factor (HRF) and molecular vibrations of PtODP.

Table S4. Comparison of photophysical and electrochemical properties of Pt(II) complexes

	λ_{PL} (nm) [a]	λ_{PL} (nm)/FWHM (nm)/S_M [b]	Φ_{PL}/τ (μs) [c]	E_{T1} (eV) [d]	HOMO/LUMO/E_g (eV) [e]
PtON-TBBI	445.8	456.0/25.1/0.467	89%/2.01	2.78	−5.35/−2.09/3.26
PtODP	453.0	458.6/16.0/0.278	95%/3.67	2.74	−5.30/−2.12/3.18

[a] Measured in 2-MeTHF at 77 K. [b] Measured in dichloromethane at room temperature. S_M, Huang–Rhys factor. [c] Measured in thermally evaporated 8 wt.% Pt(II) emitter:65 wt.% SiCzCz:27 wt.% SiTrzCz2 film, excitation wavelength = 340 nm. [d] Estimated from phosphorescent spectrum at 77 K, $E_{T1} = 1240/\lambda_{PL}$. [e] Calculated from redox potentials, HOMO = −(E_{ox} + 4.8) eV, LUMO = −(E_{red} + 4.8) eV.

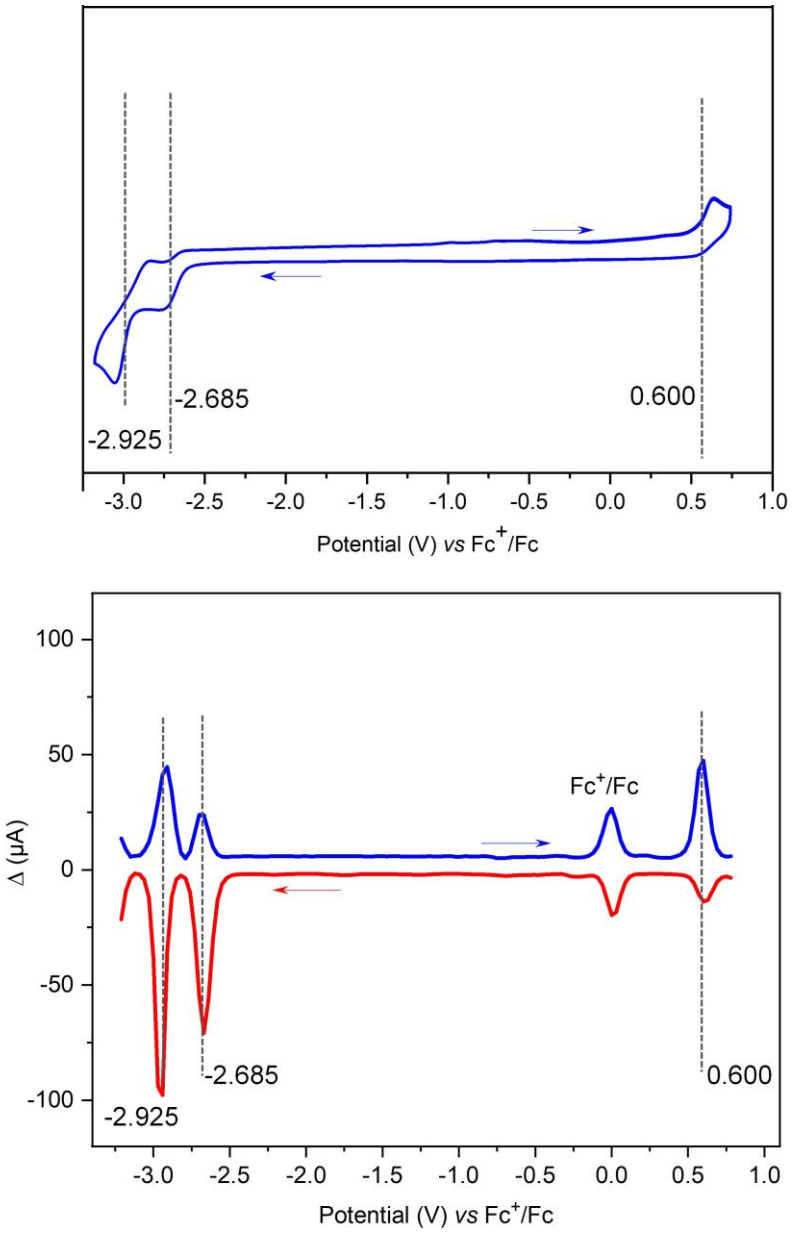

Fig. S9. Electrochemical properties of PtODP. Cyclic voltammogram (CV) and differential pulse voltammetry (DPV) of PtODP in anhydrous *N*, *N*-dimethylformamide (DMF) under nitrogen atmosphere.

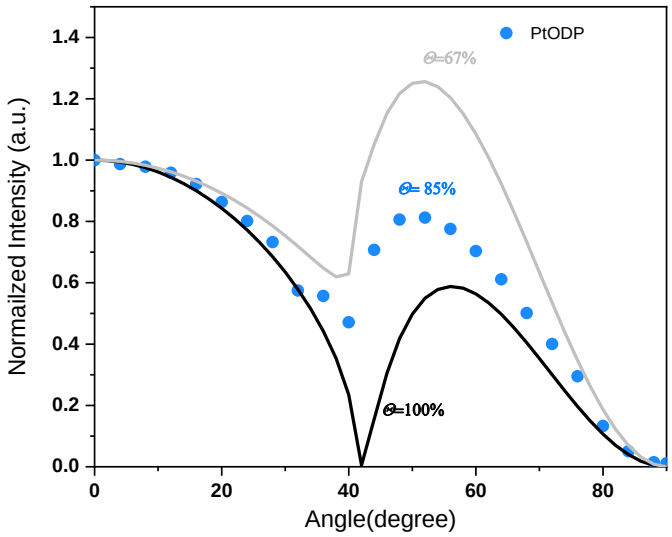

Fig. S10. Angle-dependent *p*-polarized PL spectra. Experimentally measured angle dependent *p*-polarized PL spectra of PtODP in SiCzCz: SiTrzCz2 films, and simulated curves with 100% (black) and 67% (gray) dipole orientation ratios (Θ). The doped SiCzCz: SiTrzCz2 films were fabricated by vacuum thermal evaporation.

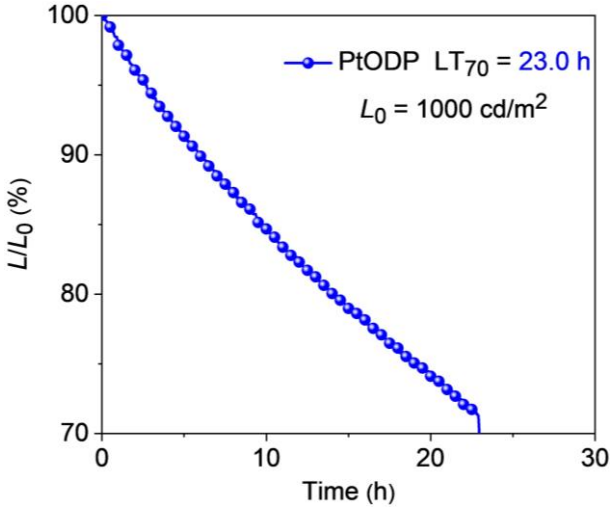

Fig. S11. The operational lifetimes of OLEDs based on Pt(II) emitters with a doping concentration of 8 wt.% at an L_0 of 1000 cd/m^2.

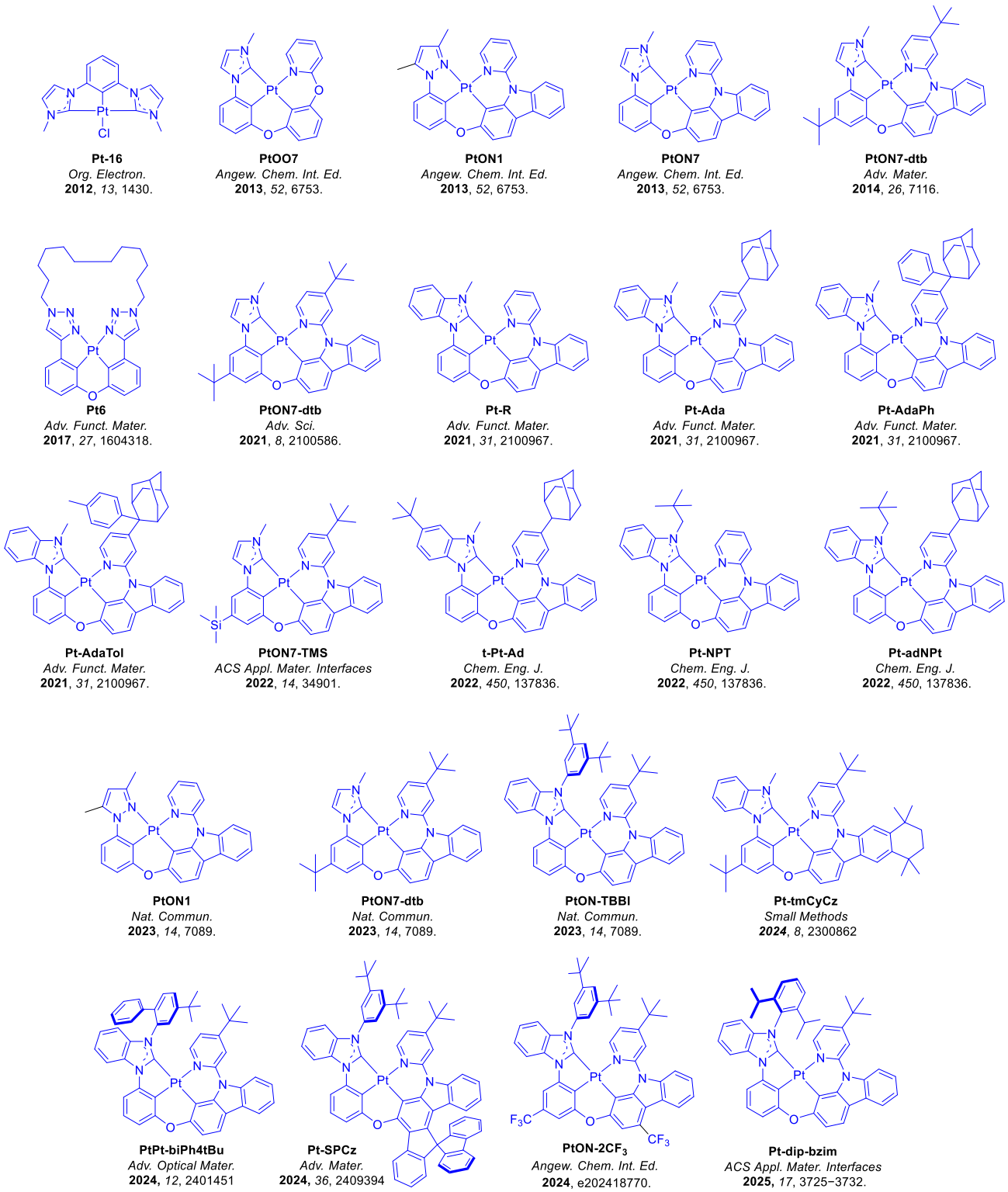

Fig. S12. Pt(II) complexes-based deep-blue emitters. Chemical structures of dopants for Pt(II)-based deep-blue phosphorescent OLEDs discussed in this work.

Table S5. Device performance data for Pt(II)-based single-layer deep-blue phosphorescent OLEDs with CIE_y < 0.15

emitter/host	CIE (x, y)	λ_{EL} (nm)/ FWHM (nm)	L_{max} (cd/m^2)	EQE (%) [a] Max/1000/5000	reference/year
PtODP/SiCzCz:SiTrzCz2 [b]	(0.129, **0.126**)	**464/19**	**84895**	**32.6/29.4/26.9**	**This work**
Pt-16/26mCPy	(0.16, 0.13)	450/~45	----	15.7/<5/----	[1]/2012
PtOO7/26mCPy	(0.15, 0.10)	448/~50	----	<9/0.5/----	[2]/2013
PtON1/26mCPy	(0.15, 0.13)	454/~49	----	25.2/16.8/----	[2]/2013
PtON7/26mCPy	(0.15, 0.14)	456/~51	----	23.7/15.4/----	[2]/2013
PtON7-dtb/TAPC:PO15	(0.148, 0.079)	452/29	1555	24.8/11.0/----	[3]/2014
Pt6/BCPO	(0.14, 0.14)	452/---	10676	9.7/7.6/5.5	[4]/2017
Pt-R/mCP	(0.138, 0.122)	~453/~37	1645	22.0/17.0/----	[5]/2021
Pt-Ada/mCP	(0.145, 0.110)	~451/~25	1078	21.2/14.5/----	[5]/2021
Pt-AdaPh/mCP	(0.137, 0.122)	~453/~37	4528	23.5/16.5/----	[5]/2021
Pt-AdaTol/mCP	(0.140, 0.120)	~453/~27.5	1593	22.0/15.5/----	[5]/2021
PtON7-TMS/mCBP	(0.142, 0.099)	452/30	2722	15.6/10.7/----	[6]/2022
t-Pt-Ad/mCP	(0.141, 0.092)	~453/~24	3258	20.3/6.3/----	[7]/2022
Pt-NPT/mCP	(0.139, 0.118)	~451/~37.5	3389	19.8/19.8/----	[7]/2022
Pt-adNPT/mCP	(0.143, 0.090)	~453/~24	2512	15.7/11.2/----	[7]/2022
PtON7-tBu/oCBP:CNmCBP-CN	(0.142, 0.143)	~452/~45	----	14.7/11.8/----	[8]/2022
PtON-TBBI/oCBP:CNmCBP-CN	(0.132, 0.147)	~453/~37	----	26.4/23.7/----	[8]/2022
PtON1/BO1b/26mCPy	(0.138, 0.130)	454/50	12982	24.8/20.9/15.0	[9]/2023
PtON1/BO1b/mCBP	(0.138, 0.142)	456/51	15722	27.1/21.8/15.6	[9]/2023
PtON7-dtb/BO1b/mCBP	(0.138, 0.088)	453/28	5670	27.6/16.0/7.9	[9]/2023
PtON-TBBI/BO1b/mCBP	(0.134, 0.104)	458/21	9377	28.0/19.0/13.4	[9]/2023
PtON-TBBI/BO2/mCB	(0.135, 0.103)	458/21	14481	22.2/14.9/10.4	[9]/2023
PtON-TBBI/BO3a/mCBP	(0.134, 0.107)	459/22	15765	19.6/14.8/10.8	[9]/2023
PtON-TBBI/BO6/mCBP	(0.133, 0.111)	459/22	10071	21.7/13.4/8.7	[9]/2023
Pt-tmCyCz/oCBP:CNmCBP-CN	(0.132, 0.138)	462/24	----	21.5/20.5/18	[10]/2024
Pt-biPh4tBu/SiBCz:SiTrzCz2	(0.139, 0.149)	461/21	~45000	21.8/19.9/16.4	[11]/2024
Pt-SPCz/SiBCz:SiTrzCz2	(0.141, 0.131)	461/22	----	25.1/21.1/18	[12]/2024
Pt-2CF3/SiBCz:SiTrzCz2	(0.140, 0.140)	461/18	48726	27.6/26.7/----	[13]/2024
Pt-dip-bzim/3-CzPB	(0.139, 0.090)	455/17	----	24.1/19.6/~12	[14]/2025

[a] EQE @ Max/1000/5000 cd m^{-2}. [b] Device structure: ITO/HATCN (20 nm)/TAPC (60 nm)/SiCzCz (5 nm)/PtQS1:SiCzCz:SiTrzCz2 (8:65:27, 35 nm)/mSiTrz (5 nm)/mSiTrz:Liq (50:50, 31 nm)/LiF (1.5 nm)/Al.

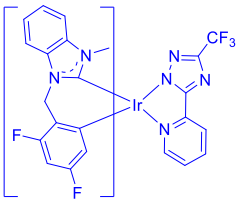

[(dfbmb)$_2$Ir(fptz)]
Angew. Chem. Int. Ed.
2008, *47*, 4512.

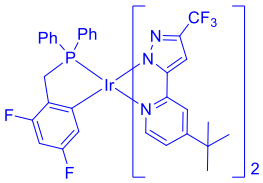

Ir(fppz)$_2$(dfbdp)
Adv. Mater.
2009, *21*, 2221.

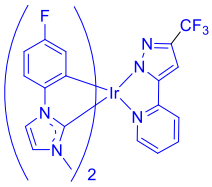

Ir(fpmi)$_2$(tfpypz)
Chem. Eur. J.
2011, *17*, 9180

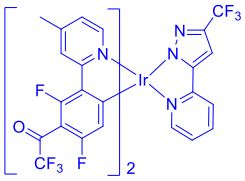

(TF)$_2$Ir(fptc)
J. Am. Chem. Soc.
2013, *135*, 14321.

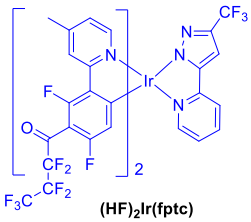

(HF)$_2$Ir(fptc)
J. Am. Chem. Soc.
2013, *135*, 14321.

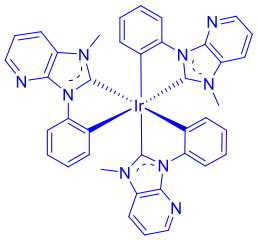

***fac*-Ir(pmp)$_3$**
Nat. Mater. **2016**, *15*, 92.

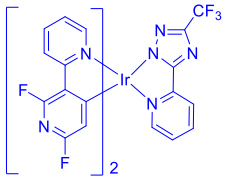

Ir1
J. Mater. Chem. C
2016, *4*, 10246.

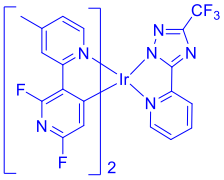

Ir2
J. Mater. Chem. C
2016, *4*, 10246.

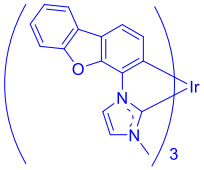

***fac*-Ir(dbfmi)$_3$**
J. Mater. Chem.C
2017, *5*, 1651.

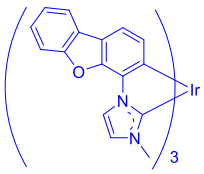

***mer*-Ir(dbfmi)$_3$**
J. Mater. Chem.C
2017, *5*, 1651.

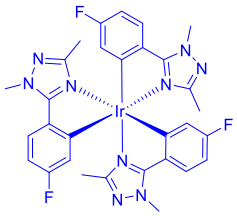

Ir(fdpt)$_3$
Adv. Mater.
2018, *30*, 1705005.

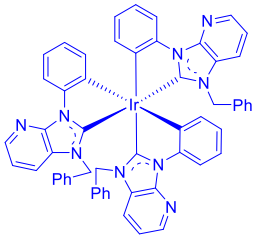

***mer*-Ir(pmp_Bn)$_3$**
Adv. Mater.
2020, *32*, 2002120.

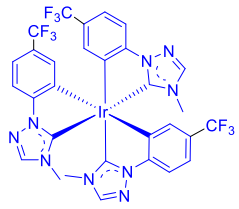

***m*-tz1**
ACS Appl. Mater. interfaces
2021, *13*, 59023.

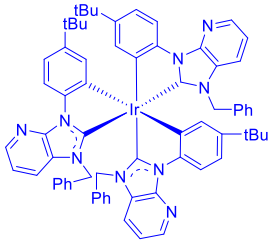

***mer*-Ir(tbpbp)$_3$**
Adv. Optical Mater.
2022, *10*, 2101686.

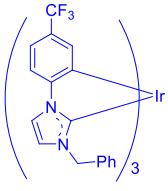

***mer*-Ir(tfpi_Bn)$_3$**
Adv. Optical Mater.
2023, *11*, 2201495.

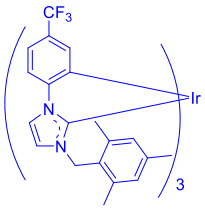

***mer*-Ir(tfpi_tmBn)$_3$**
Adv. Optical Mater.
2023, *11*, 2201495.

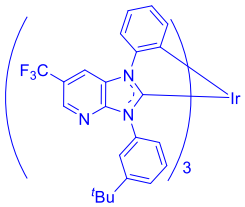

***f*-ct6a**
Adv. Mater.
2024, *36*, 2305273.

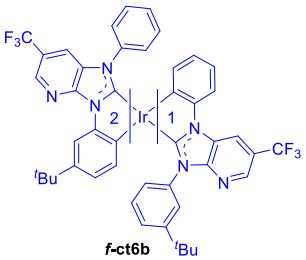

***f*-ct6b**
Adv. Mater.
2024, *36*, 2305273.

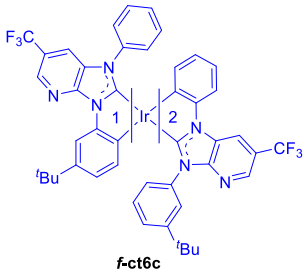

***f*-ct6c**
Adv. Mater.
2024, *36*, 2305273.

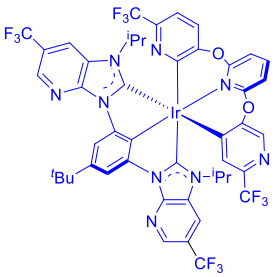

Irtb2a
ACS Appl. Mater. Interfaces
2024, *16*, 3809−3818.

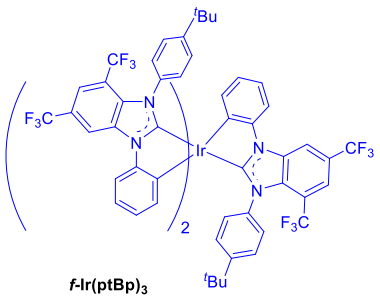

***f*-Ir(ptBp)$_3$**
Inorg. Chem. Front.
2024, *11*, 2413–2426.

Fig. S13. Ir(III) complexes-based deep-blue emitters. Chemical structures of dopants for Ir(III)-based deep-blue phosphorescent OLEDs discussed in this work.

Table S6. Device performance data for Ir(III)-based single-layer deep-blue phosphorescent OLEDs with CIE_y < 0.15

emitter/host	CIE (x, y)	λ_{EL} (nm)/ FWHM (nm)	L_{max} (cd/m^2)	EQE (%) [a] max/1000/5000	reference /year
PtODP/SiCzCz:SiTrzCz2 [b]	(0.129, **0.126**)	**464/19**	**84895**	**32.6/29.4/26.9**	**This work**
Ir(dfbmb)$_2$(fptz)/UGH2	(0.16, 0.13)	434/----	<10000	6.0/~1/----	[15]/2008
Ir(fppz)$_2$(dfbdp)/UGH2:CzSi	(0.15, 0.11)	----/----	1817	11.9/<1/----	[16]/2009
Ir(fpmi)$_2$(tfpypz)/UGH2:CzSi	(0.14, 0.10)	454/>50	3446	7.6/<6/----	[17]/2011
(TF)$_2$Ir(fptc)/mCPPO1	(0.15, 0.12)	448/>25	<2000	8.4/----/----	[18]/2013
(HF)$_2$Ir(fptc)/mCPPO1	(0.15, 0.13)	448/>25	<400	8.4/----/----	[18]/2013
fac-Ir(pmp)$_3$/TSPO1	(0.16, 0.09)	~426/~70	>7800	10.5/9.0/7.2	[19]/2016
Ir1/*t*-BuCPO	(0.15, 0.13)	430/>25	5080	11.2/8.3/4.0	[20]/2016
Ir2/*t*-BuCPO	(0.14, 0.11)	440/>25	4710	13.0/10.1/4.0	[20]/2016
fac-Ir(dbfmi)$_3$/TSPO1	(0.14, 0.11)	----/----	<2000	18.5/----/----	[21]/2017
mer-Ir(dbfmi)$_3$/TSPO1	(0.14, 0.14)	----/----	----	18.2/----/----	[21]/2017
fac-Ir3/DPEPO	(0.15, 0.05)	430/63	<500	13.4/----/----	[22]/2018
Ir(fdpt)$_3$(10 wt%)/DPEPO	(0.15, 0.11)	458/>50	2727	22.5/11.1/----	[23]/2018
Ir(fdpt)$_3$(12 wt%)/DPEPO	(0.15, 0.11)	458/>50	3195	19.4/12.6/----	[23]/2018
mer-Ir(pmp_Bn)$_3$/TSPO1	(0.149, 0.085)	445/----	6453	24.8/13.1/9.5	[24]/2020
m-tz1/DPEPO	(0.15, 0.06)	432/66	----	10.0/-----/----	[25]/2021
mer-Ir(tbpbp)$_3$/DPEPO	(0.16, 0.13)	449/>50	2386	24.9/<10/----	[26]/2022
mer-Ir(tfpi_Bn)$_3$/TSPO1	(0.16, 0.08)	424/66	632	12.2/<5/----	[27]/2023
mer-Ir(tfpi_tmBn)$_3$/TSPO1	(0.16, 0.08)	424/66	940	14.9/<5/----	[27]/2023
f-ct6a/PPF	(0.15, 0.12)	460/59	----	18.9/13.4/9.0	[28]/2024
f-ct6b/PPF	(0.14, 0.12)	456/57	----	23.4/17.1/13.0	[28]/2024
f-ct6c/PPF	(0.14, 0.13)	460/60	----	20.1/16.3/12.0	[28]/2024
Irtb2b/DPEPO	(0.15, 0.12)	456/72	----	14.8/5.7/----	[29]/2024
f-Ir(ptBp)$_3$/PPT	(0.15, 0.10)	453/57	----	12.9/6.5/3.9	[30]/2024

[a] EQE @ Max/1000/5000 cd m^{-2}. [b] Device structure: ITO/HATCN (20 nm)/TAPC (60 nm)/SiCzCz (5 nm)/PtQS1:SiCzCz:SiTrzCz2 (8:65:27, 35 nm)/mSiTrz (5 nm)/mSiTrz:Liq (50:50, 31 nm)/LiF (1.5 nm)/Al.

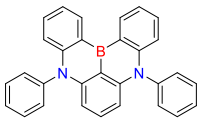

DABNA-1
Adv. Mater.
2016, *28*, 2777.

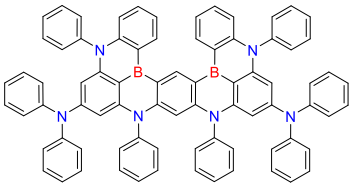

***v*-DABNA**
Nature Photon.
2019, *13*, 678–682

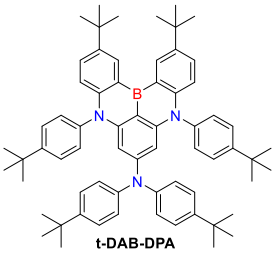

t-DAB-DPA
Mater. Today Energy
2021, 21, 100792.

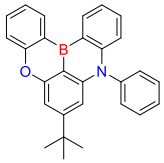

B-O-dpa
ACS Appl. Mater. Interfaces
2021, *13*, 45798.

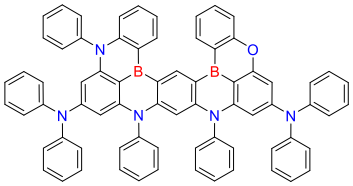

***v*-DABNA-O-OMe**
Angew. Chem., Int. Ed.
***2021**, 60, 17910–17914.*

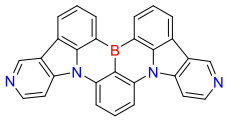

γ-Cb-B
Angew. Chem., Int. Ed.
2021, *60*, 23142–23147.

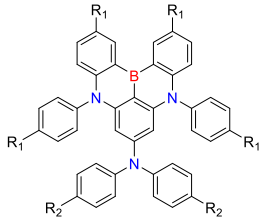

PAB (R_1,R_2=H)
2tPAB (R_1=*t*-Bu,R_2=H)
3tPAB (R_1,R_2=*t*-Bu)
Org. Electron.
2021, *97*, 106275.

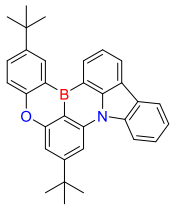

CzBNO
Adv. Opt. Mater.
2022, *10*, 2102092.

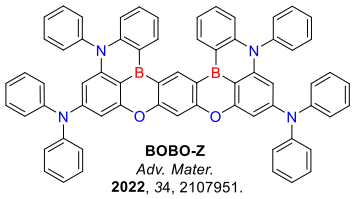

BOBO-Z
Adv. Mater.
2022, *34*, 2107951.

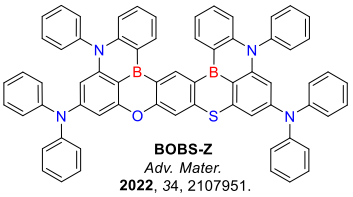

BOBS-Z
Adv. Mater.
2022, *34*, 2107951.

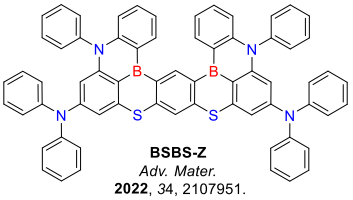

BSBS-Z
Adv. Mater.
2022, *34*, 2107951.

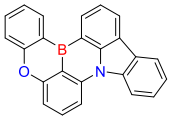

CzBO
Angew. Chem., Int. Ed.
2022, *61*, e202205684.

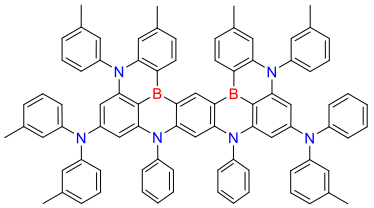

m-*v*-DABNA
Chem. Eng. J.
2022, *432*, 134381.

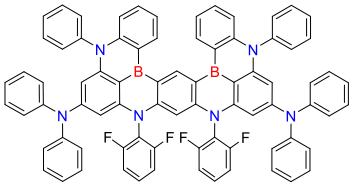

***4F-v*-DABNA**
Chem. Eng. J.
2022, *432*, 134381.

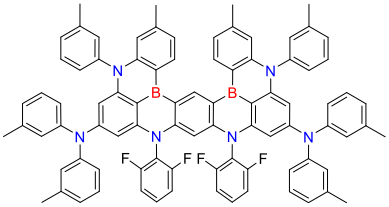

***4F-m-v*-DABNA**
Chem. Eng. J.
2022, *432*, 134381.

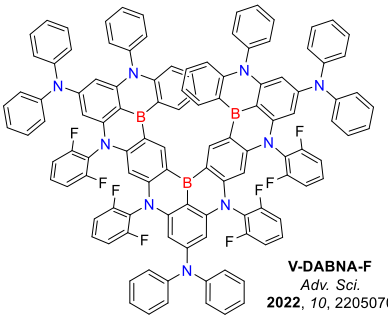

V-DABNA-F
Adv. Sci.
2022, *10*, 2205070.

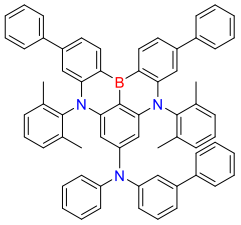

mBP-DABNA-Me
Small
2022, *18*, 2107574.

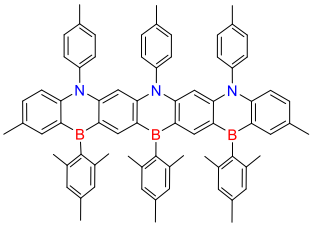

α-3BNMes
Adv. Opt. Mater.
2022, *10*, 2200688.

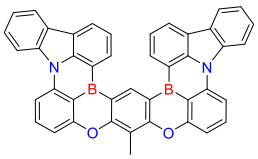

m-DINBO
Chem. Eur. J.
2022, *28*, e202201605.

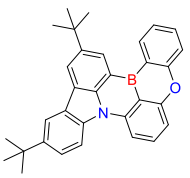

NBO
Chem. Eur. J.
2022, *28*, e202201605.

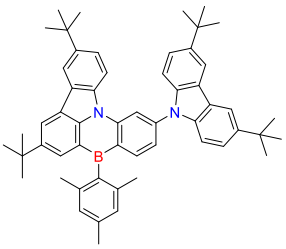

BIC-mCZ
Angew. Chem. Int. Ed.
2022, *61*, e202206916.

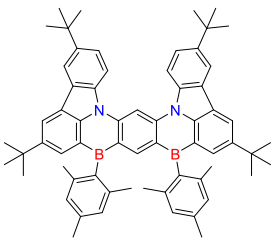

mDBIC
Angew. Chem. Int. Ed.
2022, *61*, e202206916.

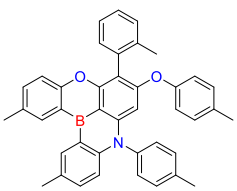

1B-DTACrs
Chem. Commun.
2022, *58*, 9377−9380.

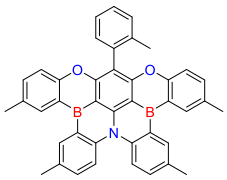

2B-DTACrs
Chem. Commun.
2022, *58*, 9377−9380.

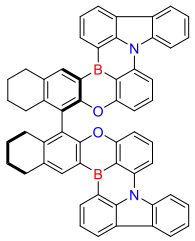

R-DOBN
Adv. Mater.
2022, *34*, 2204253.

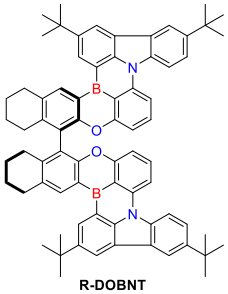

R-DOBNT
Adv. Mater.
2022, *34*, 2204253.

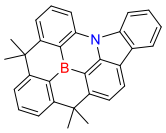

BN4
Front. Chem.
2022, *10*, 990918.

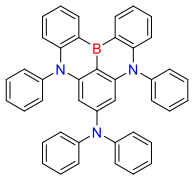

PAB
J. Mater. Chem. C.
2023, *11*, 6429−6437.

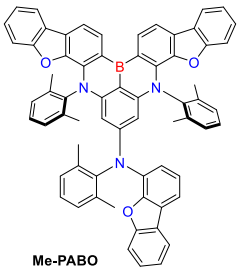

Me-PABO
J. Mater. Chem. C.
2023, *11*, 6429−6437.

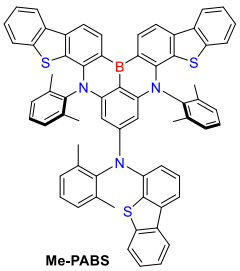

Me-PABS
J. Mater. Chem. C.
2023, *11*, 6429−6437.

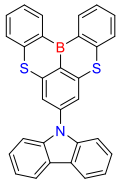

BSS-Cz
Chem. Eng. J.
2023, *451*, 138545.

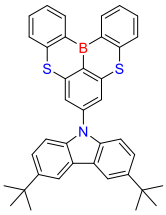

BSS-TBCz
Dyes Pigments.
2023, *220*, 111678.

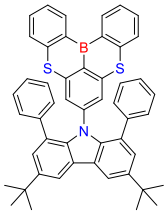

BSS-Ph-TBCz
Dyes Pigments.
2023, *220*, 111678.

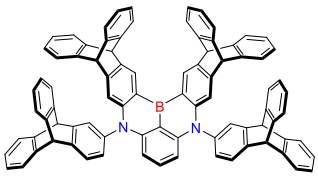

Tp-DABNA
Angew. Chem. Int. Ed.
2023. *62*, e202306879.

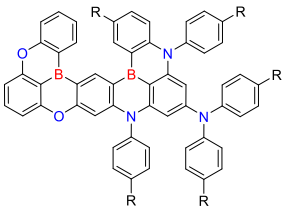

TPD4PA (R=H)
tBu-TP4PA (R=*t*Bu)
Chem. Eng. J.
2023, *451*, 138498.

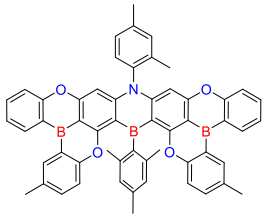

MesB-DIDOBNA-N
Adv. Mater.
2023, 2300997.

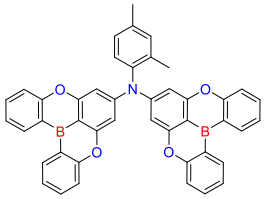

DIDOBNA-N
Adv. Mater.
2023, 2300997.

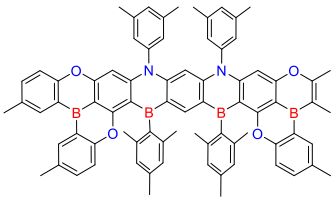

NOBNzcene
Angew. Chem., Int. Ed.
2023, *62*, e202215522.

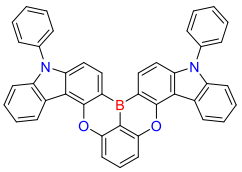

B-2OCz
Adv. Opt. Mater.
2023, 2301626

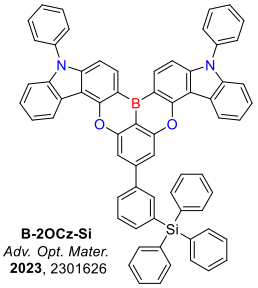

B-2OCz-Si
Adv. Opt. Mater.
2023, 2301626

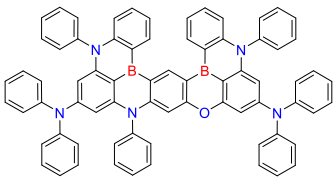

NO-DBMR
Angew. Chem., Int. Ed.
2023, e202306768.

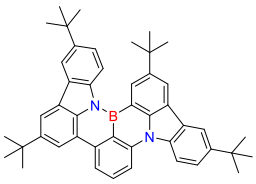

[B-N]N
Chem. Sci.
2023, *14*, 979–986.

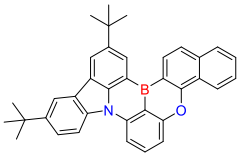

SNA
Chem. Eur. J.
2023, *29*, e202301931.

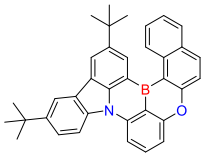

SNB
Chem. Eur. J.
2023, *29*, e202301931.

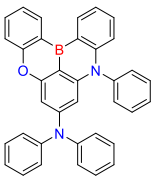

OBN
Angew. Chem., Int. Ed.
2023, **e202218947.**

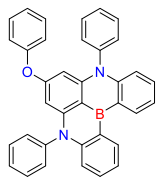

NBN
Angew. Chem., Int. Ed.
2023, **e202218947**

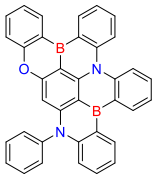

OOBN
Angew. Chem., Int. Ed.
2023, **e202218947.**

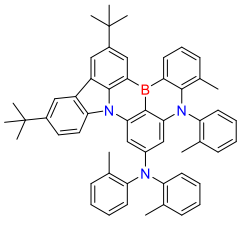

A-BN
Materials Today.
2024, 73, 30-37.

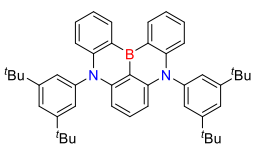

BuDABNA
Adv. Sci.
2024, 2309016.

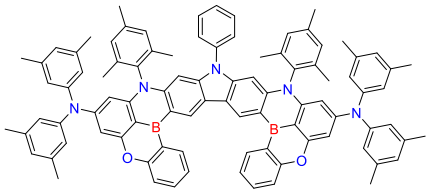

CFDBO
Adv. Optical Mater.
2024, 2302987.

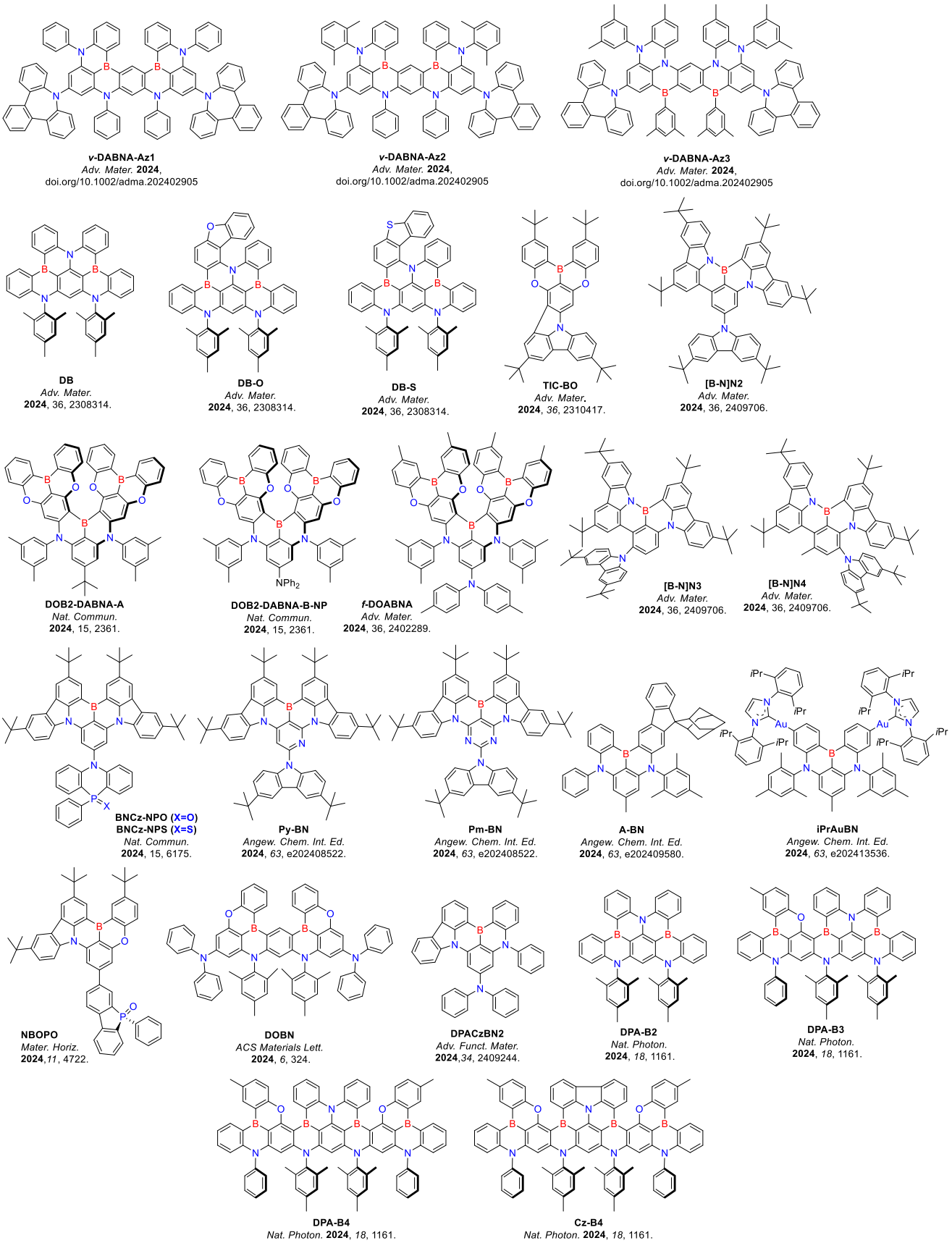

Fig. S14. Organic boron-nitrogen (BN) compounds-based deep-blue multiple resonance (MR) emitters.

Chemical structures of dopants for BN-based deep-blue MR-OLEDs discussed in this work.

Table S7. Device performance data for BN-based single-layer deep-blue MR-OLEDs with CIE_y < 0.15

emitter/host	CIE (x, y)	λ_{EL} (nm)/ HWFM (nm)	L_{max} (cd/m^2)	EQE(%) [a] max/1000/5000	reference/year
PtODP/SiCzCz:SiTrzCz2 [b]	(0.129, **0.126**)	**464/19**	**84895**	**32.6/29.4/26.9**	**This work**
DABNA-1/mCBP	(0.13, 0.09)	459/28	<1000	13.5/----/----	[31]/2016
v-DABNA/DOBNA-OAr	(0.12, 0.11)	469/18	----	34.4/26.0/----	[32]/2019
t-DAB-DPA/mCBP:mCBP-CN	(0.13, 0.08)	459/26	----	27.9/8.1/<6	[33]/2021
B-O-dpa/DPEPO	(0.15, 0.05)	443/32	<1000	16.3/----/----	[34]/2021
v-DABNA-O-Me/DOBNA-Tol	(0.13, 0.10)	465/23	<20000	29.5/26.9/----	[35]/2021
γ-Cb-B/mCBP	(0.13, 0.13)	461/28	<3000	19.0/7.7/----	[36]/2021
3tPAB/mCP	(0.14, 0.08)	460/26	1100	19.3/<5.0/----	[37]/2021
PAB/mCP	(0.14, 0.08)	456/31	782	14.7/<5.0/----	[37]/2021
2tPAB/mCP	(0.14, 0.08)	456/27	1241	16.8/<5.0/----	[37]/2021
BFCz-DABNA/mCBP-CN	(0.13, 0.09)	463/26	----	28.0/5.1/----	[38]/2022
*p*BP-DABNA-Me/mCBP:DPEPO	(0.13, 0.09)	464/23	<1200	23.4/3.2/----	[39]/2022
CzBNO/26DCzPPy	(0.14, 0.08)	454/36	----	13.6/5.5/2.0	[40]/2022
CzBO/mCBP	(0.15, 0.05)	448/30	<2000	13.4/3.5/----	[41]/2022
BOBO-Z/mCBP	(0.15, 0.04)	445/18	<2000	13.6/3.3/----	[42]/2022
BOBS-Z/mCBP	(0.14, 0.06)	456/23	<4000	26.9/15.0/----	[42]/2022
BSBS-Z/mCBP	(0.13, 0.08)	463/22	<5000	26.8/15.9/----	[42]/2022
m-*v*-DABNA/DBFPO	(0.12, 0.12)	471/18	~2000	36.2/10.2/----	[43]/2022
4F-*ν*-DABNA/DBFPO	(0.13, 0.08)	464/18	800	35.8/----/----	[43]/2022
4F-m-*ν*-DABNA/DBFPO	(0.13, 0.06)	461/18	700	33.7/----/----	[43]/2022
v-DABNA-F/DOBNA-Tol	(0.12, 0.10)	468/15	----	26.6/23.4/----	[44]/2022
mBP-DABNA-Me/mCP:DPEPO	(0.12, 0.14)	468/28	<1500	24.3/----/----	[45]/2022
α-3BNMes/DPEPO	(0.18, 0.08)	443/49	----	----/----/----	[46]/2022
m-DiNBO/mCBP	(0.13, 0.10)	466/21	<1000	24.2/----/----	[47]/2022
NBO/mCBP	(0.14, 0.14)	459/45	<1000	16.8/----/----	[47]/2022
BIC-mCz/PPF	(0.16, 0.05)	432/32	----	19.4/3.0/----	[48] /2022
mDBIC/PPF	(0.16, 0.05)	431/42	----	13.5/----/----	[48] /2022
1B-DTACrs/mCBP	(0.154, 0.049)	440/30	----	1.31/----/----	[49] /2022
2B-DTACrs/mCBP	(0.150, 0.044)	447/26	----	14.8/----/----	[49] /2022
R-DOBN /2,6-DCzPPy	(0.14, 0.10)	459/38	<10000	23.9/8.6/----	[50]/2022
R-DOBNT/2,6-DCzPPy	(0.13, 0.12)	464/35	<10000	25.6/8.6/----	[50]/2022
BN4/DPEPO	(0.17, 0.04)	423/31	----	9.1/----/----	[51]/2022
PAB/PPF	(0.147, 0.052)	452/30	1540	13.1/----/----	[52]/2023
PAB/PPF	(0.138, 0.075)	456/30	1612	15.3/----/----	[52]/2023
PAB/PPF	(0.138, 0.073)	456/30	1651	15.1/----/----	[52]/2023
Me-PABO/PPF	(0.134, 0.089)	460/26	984	20.4/----/----	[52]/2023
Me-PABS/PPF	(0.121, 0.139)	468/32	2300	23.0/3.01/----	[52]/2023
BSS-Cz/mCBP	(0.13, 0.07)	462/27	2372	20.0/----/----	[53]/2023
BSS-Cz/mCBP	(0.13, 0.09)	464/29	3257	21.8/----/----	[53]/2023
BSS-TBCz/mCBP	(0.13, 0.07)	460/34	----	19.9/----/----	[54]/2023

BSS-Ph-TBCz/mCBP	(0.12, 0.11)	468/31	----	20.7/----/----	[54]/2023
Tp-DABNA/mCBP:DPEPO	(0.14, 0.10)	462/25	----	24.3/----/----	[55]/2023
TPD4PA/mCBP-CN	(0.14, 0.06)	455/29	----	30.7/17.8/----	[56]/2023
tBu-TPAD4PA/mCBP-CN	(0.14, 0.07)	460/29	----	32.5/20.5/----	[56]/2023
MesB-DIDOBNA-N/CzSi:TSPO1	(0.17, 0.05)	402/21	<1000	16.2/----/----	[57]/2023
DIDOBNA-N/TSPO1	(0.15, 0.07)	429/70	<1000	15.2/----/----	[57]/2023
NOBNacene/TSPO1	(0.17, 0.06)	409/37	<100	8.5/----/----	[58]/2023
B-2OCz/DPEPO	(0.15, 0.06)	432/70	<1000	8.4/----/----	[59]/2023
B-2OCz-Si/DPEPO	(0.16, 0.04)	423/49	<1000	15.2/----/----	[59]/2023
NO-DBMR/DBFPO	(0.12, 0.12)	469/26	----	33.7/<20/----	[60]/2023
[B-N]N/mCBP	(0.15, 0.08)	448/27.3	2002	16.7/7.6/----	[61]/2023
SNA/PPF	(0.14, 0.11)	460/38	985	7.2/----/----	[62]/2023
SNB/PPF	(0.13, 0.12)	466/32	1648	7.9/<1/----	[62]/2023
OBN/DBFDPO	(0.15, 0.09)	437/44	----	15.7/----/----	[63]/2023
ODBN/DBFDPO	(0.15, 0.10)	446/54	----	24.15/~5/----	[63]/2023
NBN/DBFDPO	(0.14, 0.09)	452/40	----	23.02/~6/----	[63]/2023
A-BN/mCBP	(0.13, 0.08)	462/24	----	41.5/10.4/----	[64]/2024
BuDABNA/SiCzCz:SiTrzCz2	(0.14, 0.09)	460/27	----	25.1/----/----	[65]/2024
CFDBO/mCBP	(0.14, 0.12)	460/24	8985	20.7/<10/<5	[66]/2024
v-DABNA/DOBNA-OAr	(0.12, 0.12)	469/18	----	33.8/25.1/----	[67]/2024
v-DABNA-Az1/DOBNA-OAr	(0.14, 0.08)	459/~19	----	30.8/19.9/----	[67]/2024
v-DABNA-Az2/DOBNA-OAr	(0.14, 0.06)	458/~18	----	29.9/16.0/----	[67]/2024
v-DABNA-Az3/DOBNA-OAr	(0.14, 0.10)	459/~19	----	33.0/22.4/----	[67]/2024
DB/ DOBNA-OAr	(0.154, 0.048)	443/26	10486	23.4/9.0/5.5	[68]/2024
(*P*)-DB-O/DOBNA-OAr	(0.150, 0.041)	445/24	11610	27.5/11.4/6.8	[68]/2024
(*M*)-DB-S/DOBNA-OAr	(0.148, 0.047)	447/24	11153	29.3/12.2/6.0	[68]/2024
TIC-BO/CzSi	(0.160, 0.050)	428/43	346	20.5/----/----	[69]/2024
DOB-DABNA-A/DOBNA-Tol	(0.145, 0.049)	452/24	----	23.3//21.6/----	[70]/2024
DOB-DABNA-B-NP/DOBNA-Tol	(0.117, 0.127)	471/23	----	27.4//24.0/----	[70]/2024
f-DOABNA/DOBNA-Tol	(0.153, 0.056)	445/28	4858	19.9/6.7/----	[71]/2024
[B-N]N2/SiCzCz:SiTrzCz2	(0.152, 0.046)	441/20	8714	20.3/----/----	[72]/2024
[B-N]N3/SiCzCz:SiTrzCz2	(0.141, 0.105)	459/40	19520	19.6/----/----	[72]/2024
[B-N]N4/SiCzCz:SiTrzCz2	(0.134, 0.133)	466/30	29960	22.1/----/----	[72]/2024
Py-BN/DOBNA-OAr	(0.153, 0.045)	444/21	1967	15.8/3.9/----	[73]/2024
Pm-BN/DOBNA-OAr	(0.161, 0.045)	415/24	1261	5.8/2.5/----	[73]/2024
A-BN/*p*-PhBCzPh	(0.129, 0.105)	464/23	3259	24.8/4.8/----	[74]/2024
iPrAuBN/mCP	(0.154, 0.036)	442/19	----	14.8/----/----	[75]/2024
NBOPO/mCBP	(0.13, 0.12)	468/31	2709	16.4/2.51/----	[76]/2024
DOBN/mCBP	(0.15, 0.04)	449/20	1231	35.4/----/----	[77]/2024
DPA-B2/SiCzCz:SiTrzCz2	(0.153, 0.055)	444/31	21620	28.9/9.3/----	[78]/2024
DPA-B3/SiCzCz:SiTrzCz2	(0.150, 0.043)	450/15	24637	37.7/21.0/----	[78]/2024
DPA-B4/SiCzCz:SiTrzCz2	(0.141, 0.050)	457/14	27911	39.2/28.7/----	[78]/2024
Cz-B4/SiCzCz:SiTrzCz2	(0.138, 0.076)	457/26	27428	32.1/16.1/----	[78]/2024

[a] EQE @ Max/1000/5000 cd m^{-2}. [b] Device structure: ITO/HATCN (20 nm)/TAPC (60 nm)/SiCzCz (5 nm)/PtQS1:SiCzCz:SiTrzCz2 (8:65:27, 35 nm)/mSiTrz (5 nm)/mSiTrz:Liq (50:50, 31 nm)/LiF (1.5 nm)/Al.

Table S8. Device performance data for BN-based single-layer deep-blue hyperfluorescence (HF)-OLEDs with CIE_y < 0.15

sensitizer/emitter/host	CIE (x, y)	λ_{EL} (nm)/ FWHM (nm)	L_{max} (cd/m^2)	EQE(%) [a] max/1000/5000	reference /year
PtODP/SiCzCz:SiTrzCz2 [b]	(0.129, **0.126**)	**464/19**	**84895**	**32.6/29.4/26.9**	**This work**
Ir(cb)$_3$/*t*-DABNA/mCBP	(0.129, 0.108)	<480/27	----	20.2/14.2/10.0	[79]/2019
p4TCzPhBN/*t*-DABNA/DPEPO	(0.13, 0.12)	~460/29	----	32.5/23.2/----	[80]/2020
PtON7-dtb/*v*-DABNA/oCBP:mCBP-2CN	(0.111, 0.141)	473/20	----	32.2/25.4/22.5	[81]/2021
Pt-5/*v*-DABNA/mCBP	(0.13, 0.12)	469/18	13200	23.4/22.4/19.8	[82]/2021
DMAC-DPS/tDPAC-BN/DPEPO	(0.14, 0.09)	460/28	1126	21.6/5.4/----	[83]/2022
Ir-f-tpb1/*t*-DABNA/mCBP	(0.13, 0.11)	462/30	<10000	29.6/~10/<5	[84]/2022
Ir-f-CF$_3$/*t*-DABNA/mCBP	(0.13, 0.14)	464/30	8188	23.8/10.4/<10	[85]/2022
TDBA-SAF/pBP-DABNA-Me/mCBP:DPEPO	(0.133, 0.109)	462/22	----	30.1/4.8/----	[86]/2022
3Cz2BN/BN1/DPFPO	(0.14, 0.08)	457/28	8323	31.2/9.3/<8	[87]/2022
3Cz2BN/BN2/DPFPO	(0.13, 0.11)	467/23	14064	33.2/15.5/~10	[87]/2022
3Cz2BN/BN3/DBFPO	(0.14, 0.08)	458/23	18438	37.6/26.2/~16	[87]/2022
DtBuAc-DBT/*α*-3BNMes/DBFPO	(0.15, 0.10)	~460/49	<1000	15/----/----	[88]/2022
PtON-TBBI/*t*-DABNA/SiCzCz: SiTrzCz2	(----, 0.051)	----/----	----	18.4/----/----	[89]/2022
PtON-TBBI/TBE01/SiCzCz: SiTrzCz2	(----, 0.064)	----/----	----	24.2/----/----	[89]/2022
PtON-TBBI/TBE02/SiCzCz: SiTrzCz2	(----, 0.058)	----/----	----	26.6/----/----	[89]/2022
Ir-B3/*v*-DABNA/PPT	(0.116,0.114)	473/----	7823	26.2/17.9/~11.0	[90]/2022
p4TzPhBN/C-BN/MCBP	(0.14, 0.07)	453/25	----	26.6/8.9/~6	[91]/2022
TDBA-SAF/Tp-DABNA/mCBP:DPEPO[c]	(0.14, 0.13)	462/29	----	27.5/----/----	[92]2023
TDBA-SAF/*t*-DABNA/mCBP:DPEPO[c]	(0.13, 0.14)	464/34	----	23.3/----/----	[92]2023
Ir-*f*-ct6a/*v*-DABNA/PPF	(0.12, 0.13)	472/22	----	26.2/18.4/14.8	[93]/2023
Ir-*f*-ct6b/*v*-DABNA/PPF	(0.12, 0.13)	472/22	----	25.1/17.7/13.0	[93]/2023
Ir-*f*-ct6c/*v*-DABNA/PPF	(0.12, 0.13)	472/22	----	25.8/17.3/12.5	[93]/2023
Ir-*f*-ct1a/*v*-DABNA/mCBP	(0.12, 0.14)	472/21	----	22.8/22.0/19.0	[94]/2023
Ir-*f*-ct1b/*v*-DABNA/mCBP	(0.12, 0.12)	472/20	----	27.9/24.5/21.0	[94]/2023
Ir-*f*-ct1c/*v*-DABNA/mCBP	(0.12, 0.11)	472/18	----	35.5/ 24.0/20.3	[94]/2023
Ir-*f*-ct1d/*v*-DABNA/mCBP	(0.17, 0.12)	472/20	----	19.2/15.4/13.4	[94]/2023
3Cz2BN/SNA/PPF	(0.14, 0.11)	458/30	13800	29.3/~20/<15	[95]/2023
3Cz2BN/SNB/PPF	(0.14, 0.12)	462/35	14659	29.1/~20/<15	[95]/2023
CzBN/CzBN-mCP/2,6-DCzPPy	(0.13, 0.14)	469/28	15749	30.6/23.8/18.0	[96]/2023
m4TCzPhBN/DBCz-Mes/mCBP	(0.14, 0.06)	452/17	<4000	33.9/8.5/<4.0	[97]/2023
Ir-B-4-TMS/*v*-DABNA/CzSi	(0.127, 0.097)	467/18	6083	29.5/20.6/----	[98]/2023
Ir-B-5-TMS/*v*-DABNA/CzSi	(0.126,0.097)	467/18	8137	31.1/22.7/----	[98]/2023
Ir-B-4-TMS/*v*-DABNA/SiCzCz:SiTrzCz2	(0.119, 0.123)	470/17	54138	33.4/23.0/~19	[98]/2023
Ir-B-5-TMS/*v*-DABNA/SiCzCz:SiTrzCz2	(0.119, 0.123)	470/17	53037	33.4/24.1/~20	[98]/2023
D-5CzBN/*v*-DABNA/SiCzCz: SiTrzCz2	(0.14,0.14)	468/19	----	29.2/24.1/17.5	[99]/2024
Pt-dipPhCz/*v*-DABNA/SiCzCz:SiTrzCz2	(0.124, 0.116)	470/18	----	31.4/26.7/22.8	[100]/2024
Pt-tmCyCz/*v*-DABNA/SiCzCz:SiTrzCz2	(0.116, 0.123)	472/19	----	33.9/31.2/26.0	[101]/2024
Ir-*f*-ct5mix/*v*-DABNA/CzSi	(0.127, 0.098)	~465/17	8220	32.0/20.1/~19	[102]/2024

Ir-*f*-ct5mix/*v*-DABNA/SiCzCz:SiTrzCz2	(0.120, 0.132)	~470/17	30476	30.3/25.5/~20	[102]/2024
Ir-*f*-CN1/m-DINBO/mCPCN	(0.13, 0.10)	467/20	2640	30.8/14.7/----	[103]/2024
Ir-*f*-CN2/m-DINBO/mCPCN	(0.14, 0.13)	467/19	3800	30.1/15.9/----	[103]/2024
Ir-*f*-ct7a/*t*-DABNA/PPF	(0.14, 0.09)	460/26.6	4887	32.5/14.9/10.0	[104]/2024
Ir-*f*-ct7b/*t*-DABNA/PPF	(0.14, 0.09)	460/26.5	3408	36.1/13.3/----	[104]/2024
Ir-*f*-ct7c/*t*-DABNA/PPF	(0.14, 0.09)	460/27	2345	26.4/12.4/----	[104]/2024
Ir-*f*-ct9b/*v*-DABNA/SiCzCz:SiTrzCz2	(0.127, 0.123)	469/18	----	32.1/25.5/21.3	[105]/2024
p4TCzPhBN/A-BN/mCBP	(0.14, 0.09)	462/25	<2000	38.5/25.1/----	[106]/2024
f-Ir(dfpb)$_3$/*t*-DABNA/PPT	(0.13,0.12)	466/30	----	14.3/4.5/----	[107]/2024
f-Ir(tBpp)$_3$/*t*-DABNA/PPT	(0.14,0.10)	462/29	----	18.1/9.7/---	[107]/2024
f-Ir(ptBp)$_3$/*v*-DABNA/PPT	(0.12,0.13)	473/20	----	16.3/9.4/---	[107]/2024
f-Ir(ptBp)$_3$/*t*-DABNA/PPT	(0.14,0.10)	461/33	----	14.1/5.19/----	[107]/2024
PtON-TBBI/*t*-DABNA/SiCzCz:SiTrzCz2	(0.138,0.102)	460/26	----	26.1/24.3/21	[12]/2024
Pt-SPCz/*t*-DABNA/SiCzCz:SiTrzCz2	(0.136,0.096)	460/26	----	28.1/25.3/22	[12]/2024
TBCz-XT/*v*-DABNA/PPF	(0.131,0.104)	470/19	9362	24.0/13.0/----	[108]/2024
DMAC-DPS/*v*-DABNA/PPF	(0.131, 0.113)	470/18	12680	29.6/18.0/----	[108]/2024
PPCz-Trz/*v*-DABNA/PPF	(0.133, 0.128)	470/19	13030	28.6/11.8/----	[108]/2024
TBCz-XT/*t*-DABNA/PPF	(0.140, 0.104)	462/32	7588	25.0/6.4/----	[108]/2024
DMAC-DPS/*t*-DABNA/PPF	(0.135, 0.130)	462/29	7813	26.2/6.0/----	[108]/2024
PPCz-Trz/*t*-DABNA/PPF	(0.141, 0.125)	462/28	8001	25.9/5.4/----	[108]/2024
TDBA-PAS/Py-BN/DOBNA-OAr	(0.150, 0.052)	445/22	6467	27.7/16.1/----	[74]/2024
3Cz2BN/DPACzBN2/2,6-DCzPPy	(0.14, 0.13)	461/34	15180	28.5/25.2/----	[109]/2024
*m*MDBA-DI/DPA-B4/SiCzCz:SiTrzCz2	(0.142, 0.099)	459/16	41607	44.6/38.8/----	[78]/2024

[a] EQE @ Max/1000/5000 cd m^{-2}. [b] Device structure: ITO/HATCN (20 nm)/TAPC (60 nm)/SiCzCz (5 nm)/PtQS1:SiCzCz:SiTrzCz2 (8:65:27, 35 nm)/mSiTrz (5 nm)/mSiTrz:Liq (50:50, 31 nm)/LiF (1.5 nm)/Al.

Supplementary References:

[1] Fleetham T, Wang Z, Li J. Efficient deep blue electrophosphorescent devices based on platinum(II) bis(n-methyl-imidazolyl)benzene chloride. Org Electron, 2012,13: 1430−1435

[2] Hang X.-C, Fleetham T, Turner E, *et al*. Highly efficient blue-emitting cyclometalated platinum(II) complexes by Judicious molecular design. *Angew Chem Int Ed*, 2013, 52: 6753−6756

[3] Fleetham T, Li G, Wen L, *et al*. Efficient "pure" blue OLEDs employing tetradentate Pt complexes with a narrow spectral bandwidth. Adv Mater, 2014, 26: 7116−7121

[4] Wang X, Peng T, Nguyen C, *et al*. Highly efficient deep-blue electrophosphorescent Pt(II) compounds with non-distorted flat geometry: tetradentate versus macrocyclic chelate ligands. Adv Funct Mater, 2017, 27:1604318

[5] Huh J.-S, Sung MJ, Kwon S.-K, *et al*. Highly efficient deep blue phosphorescent OLEDs based on tetradentate Pt(II) complexes containing adamantyl spacer groups. Adv Funct Mater, 2021, 31: 2100967

[6] Park HJ, Jang J.-H, Lee J.-H, *et al*. Highly efficient deep-blue phosphorescent OLEDs based on a trimethylsilyl-substituted tetradentate Pt(II) complex. ACS Appl Mater Interfaces, 2022, 14: 34901–34908

[7] Huh J.-S, Lee DY, Park KH, *et al*. Control of the horizontal dipole ratio and emission color of deep blue tetradentate Pt(II) complexes using aliphatic spacer groups. Chem Eng J, 2022, 450: 137836

[8] Sun J, Ahn H, Kang S, *et al*. Exceptionally stable blue phosphorescent organic light-emitting diodes. Nat Photon, 2022, 16: 212−218

[9] Li G, Xu K, Zheng J, *et al*. Double boron–oxygen-fused polycyclic aromatic hydrocarbons: skeletal editing and applications as organic optoelectronic materials. Nat Commun, 2023, 14: 7089

[10] Cheong K, Jo U, Hong WP, *et al*. Fused cycloalkyl unit-functionalized tetradentate Pt(II) complexes for efficient and narrow-emitting deep blue organic light-emitting diodes. Small Methods, 2024, 8: 2300862

[11] Choi J, Cheong K, Han S, *et al*. Narrowband emission in Pt(II) complexes via ligand engineering for blue phosphorescent organic light-emitting diodes. Adv Opt Mater, 2024, 12: 2401451

[12] Lee H, Park B, Han GR, *et al*. Superbly efficient and stable ultrapure blue phosphorescent organic light-emitting diodes with tetradentate Pt(II) complex with vibration suppression effect. Adv Mater, 2024, 36: 2409394

[13] Zhu J, Huang M, Zhang Y, *et al*. Improving the blue color purity of tetradentate Pt(II) complexes with the assistance of F···H interaction towards high-performance blue phosphorescent OLEDs with EQE over 33%. Angew Chem Int Ed, 2024, 64: e202418770

[14] Cheong K, Han S, Lee JY. High efficiency and narrow emissions in deep-blue Pt(II) emitters in organic light-emitting diodes via anchor-shaped substituent design. ACS Appl Mater Interfaces, 2025,17: 3725−3732

[15] Chang C.-F, Cheng Y.-M, Chi Y, *et al*. Highly efficient blue-emitting iridium(III) carbene complexes and phosphorescent OLEDs. Angew Chem Int Ed, 2008,47: 4542–4545

[16] Chiu B. Y.-C, Hung J.-Y, Chi Y, *et al*. En route to high external quantum efficiency (~12%), organic true-blue-light-emitting diodes employing novel design of iridium (III) phosphors. Adv Mater, 2009, 21: 2221–2225

[17] Hsieh C.-H, Wu F.-I, Fan C.-H, *et al*. Design and synthesis of iridium bis (carbene) complexes for efficient blue electrophosphorescence. Chem Eur J, 2011, 17: 9180–9187

[18] Lee S, Kim S.-O, Shin H, *et al*. Deep-blue phosphorescence from perfluoro carbonyl-substituted iridium complexes. J Am Chem Soc, 2013, 135: 14321−14328

[19] Lee J, Chen H.-F, Batagoda T, *et al*. Deep blue phosphorescent organic light-emitting diodes with very high brightness and effciency. Nat Mater, 2016, 15: 92–98

[20] Feng Y, Zhuang X, Zhu D, *et al*. Rational design and characterization of heteroleptic phosphorescent iridium(III) complexes for highly efficient deep-blue OLEDs. J Mater Chem C, 2016, 4: 10246–10252

[21] Cho Y.-J, Kim S.-Y, Kim J.-H, *et al*. Probing photophysical properties of isomeric *N*-heterocyclic carbene Ir(III) complexes and their applications to deep-blue phosphorescent organic light-emitting diodes. J. Mater Chem C, 2017, 5: 1651−1659

[22] Pal AK, Krotkus S, Fontani M, *et al*. High-efficiency deep-blue-emitting organic light-emitting diodes based on iridium(III) carbene complexes. Adv Mater, 2018, 30: 1804231

[23] Li X, Zhang J, Zhao Z, *et al*. Deep blue phosphorescent organic light-emitting diodes with CIE_y value of 0.11 and external quantum efficiency up to 22.5%. Adv Mater, 2018, 30: 1705005

[24] Park H.-Y, Maheshwaran A, Moon C.-K, *et al*. External quantum efficiency exceeding 24% with CIE_y value of 0.08 using a novel carbene-based iridium complex in deep-blue phosphorescent organic light-emitting diodes. Adv Mater, 2020, 32: 2002120

[25] You C, Wang X.-Q, Zhou X, *et al*. Homoleptic Ir(III) phosphors with 2-phenyl-1,2,4-triazol-3-ylidene chelates for efficient blue organic light-emitting diodes. ACS Appl Mater Interfaces, 2021, 13: 59023–59034

[26] Kumaresan R, Park H.-Y, Maheshwaran A, *et al*. High performance solution-processed deep-blue phosphorescence organic light-emitting diodes with EQE over 24% by employing new carbenic Ir(III) complexes. Adv Opt Mater, 2022, 10: 2101686

[27] Mackenzie CFR, Zhang L, Cordes DB, *et al*. Bulky iridium NHC complexes for bright, efficient deep-blue oleds. Adv Opt Mater, 2023, 11: 2201495

[28] Yan J, Feng Z.-Q, Wu Y, *et al*. Blue electrophosphorescence from iridium(III) phosphors bearing asymmetric di-*N*-aryl6-(trifluoromethyl)-2*H*-imidazo[4,5-*b*]pyridin-2-ylidene chelates. Adv Mater, 2024, 36: 2305273

[29] Yan J, Qu Z.-H, Zhou D.-Y, *et al*. Bis-tridentate Ir(III) phosphors and blue hyperphosphorescence with suppressed efficiency roll-off at high brightness. ACS Appl Mater Interfaces, 16, 2024, 3: 3809–3818

[30] Yan J, Pan Y, Peng I.-C, *et al*. Selective syntheses of homoleptic Ir(III) complexes bearing di-CF_3-functionalized benzoimidazol-2-ylidenes for generation of blue phosphorescence. Inorg Chem Front, 2024, 11: 2413–2426

[31] Hatakeyama T, Shiren K, Nakajima K, *et al*. Ultrapure blue thermally activated delayed fluorescence molecules: efficient HOMO–LUMO separation by the multiple resonance effect. Adv Mater, 2016, 28: 2777–2781

[32] Kondo Y, Yoshiura K, Kitera S, *et al*. Narrowband deep-blue organic light-emitting diode featuring an organoboron-based emitter. Nat Photon, 2019, 13: 678–682

[33] Kim JH, Chung WJ, Kim J, *et al*. Concentration quenching-resistant multiresonance thermally activated delayed fluorescence emitters. *Mater*. Today Energy, 2021, 21: 100792

[34] Park J, Lim J, Lee JH, *et al*. Asymmetric blue multiresonance TADF emitters with a narrow emission band. ACS Appl Mater Interfaces, 2021, 13: 45798–45805

[35] Tanaka H, Oda S, Ricci G, *et al*. Hypsochromic shift of multiple-resonance-induced thermally activated delayed fluorescence by oxygen atom incorporation. Hypsochromic shift of multiple-resonance-induced thermally activated delayed fluorescence by oxygen atom incorporation. Angew Chem Int Ed, 2021, 60: 17910–17914

[36] Yang M, Shikita S, Min H, *et al*. Wide-range color tuning of narrowband emission in multi-resonance organoboron delayed fluorescence materials through rational imine/amine functionalization. Angew Chem Int Ed, 2021, 60: 23142–23147

[37] Wang Y, Duan Y, Guo R, *et al*. A periphery cladding strategy to improve the performance of narrowband emitters, achieving deep-blue OLEDs with CIE_y < 0.08 and external quantum efficiency approaching 20%. Org Electron: 2021, 97: 106275

[38] Lee H, Braveenth R, Park JD, *et al*. Manipulating spectral width and emission wavelength towards highly efficient blue asymmetric carbazole fused multi-resonance emitters. ACS Appl Mater Interfaces, 2022, 14: 36927–36935

[39] Cheon H.-J, Woo S.-J, Baek S.-H, *et al*. Dense local triplet states and steric shielding of a multi-resonance TADF emitter enable high-performance deep-blue OLEDs. Adv Mater, 2022, 34: 2207416

[40] Han J, Huang Z, Lv X, *et al*. Simple molecular design strategy for multiresonance induced TADF emitter: highly efficient deep blue to blue electroluminescence with high color purity. Adv Op. Mater, 2022, 10: 2102092

[41] Park IS, Min H, Yasuda T. Ultrafast triplet–singlet exciton interconversion in narrowband blue organoboron emitters doped with heavy chalcogens. Angew Chem Int Ed, 2022, 61: e202205684

[42] Park IS, Yang M, Shibata H, *et al*. Achieving ultimate narrowband and ultrapure blue organic light-emitting diodes based on polycyclo-heteraborin multi-resonance delayed-fluorescence emitters. Adv Mater, 2022, 34: 2107951

[43] Naveen KR, Lee H, Braveenth R, *et al*. Deep blue diboron embedded multi-resonance thermally activated delayed fluorescence emitters for narrowband organic light emitting diodes. Chem Eng J, 2022, 432: 134381

[44] Oda S, Kawakami B, Horiuchi M, *et al*. Ultra-narrowband blue multi-resonance thermally activated delayed fluorescence materials. Adv Sci, 2023, 10: 2205070

[45] Cheon HJ, Shin Y.-S, Park N.-H, *et al*. Boron-based multi-resonance TADF emitter with suppressed intermolecular interaction and isomer formation for efficient pure blue OLEDs. Small, 2022, 18: 2107574

[46] Stavrou K, Suresh SM, Hall D, *et al*. Emission and absorption tuning in TADF B,N-doped heptacenes: toward ideal-blue hyperfluorescent OLEDs. Adv Opt Mater, 2022, 10: 2200688

[47] Liu G, Sasabe H, Kumada K, *et al*. Nonbonding/bonding molecular orbital regulation of nitrogen-boron-oxygen-embedded blue/green multiresonant TADF emitters with high efficiency and color purity. Chem Eur J, 2022, 28: e202201605

[48] Wang X, Zhang Y, Dai H, *et al*. Mesityl-functionalized multi-resonance organoboron delayed fluorescent frameworks with wide-range color tunability for narrowband OLEDs. Angew Chem Int Ed, 2022, 61: e202206916

[49] Chan C.-U, Suresh SM, Lee Y.-T, *et al*. Two boron atoms versus one: high-performance deep-blue multi-resonance thermally activated delayed fluorescence emitters. Chem Commun, 2022, 58: 9377−9380

[50] Yan Z.-P, Yuan L, Zhang Y, *et al*. A chiral dual-core organoboron structure realizes dual-channel enhanced ultrapure blue emission and highly efficient circularly polarized electroluminescence. Adv Mater, 2022, 34: 2204253

[51] Bae J, Sakai M, Tsuchiya Y, *et al*. Multiple resonance type thermally activated delayed fluorescence by

dibenzo [1,4] azaborine derivatives. Front Chem, 2022, 10: 990918

[52] Di K, Guo R, Wang Y, *et al*. Achieving high-performance narrowband blue MR-TADF emitters by suppressing isomer formation and extending p-conjugate skeletons. J Mater Chem C, 2023, 11: 6429−6437

[53] Chang Y, Wu Y, Wang X, *et al*, Boron, sulfur-doped polycyclic aromatic hydrocarbon emitters with multiple-resonance-dominated lowest excited states for efficient narrowband deep-blue emission. Chem Eng J, 2023, 451: 138545

[54] Chang Y, Wu Y, Zhang K, *et al*. 1,8-Diphenyl-carbazole-based boron, sulfur-containing multi-resonance emitters with suppressed aggregation emission for narrowband OLEDs. Dyes Pigments, 2023, 220:111678

[55] Mubarok H, Amin A, Lee T, *et al*. Triptycene-fused sterically shielded multi-resonance TADF emitter enables high-efficiency deep blue OLEDs with reduced dexter energy transfer. Angew Chem Int Ed, 2023, 62: e202306879

[56] Naveen KR, Lee H, Seung LH, *et al*. Modular design for constructing narrowband deep-blue multiresonant thermally activated delayed fluorescent emitters for efficient organic light emitting diodes. Chem Eng J, 2023, 451: 138498

[57] Suresh SM, Zhang L, Matulaitis T, *et al*. Judicious heteroatom doping produces high-performancedeep-blue/near-UV multiresonant thermally activated delayed fluorescence OLEDs. Adv Mater, 2023, 2300997

[58] Suresh SM, Zhang L, Hall D, *et al*. A deep-blue-emitting heteroatom-doped MR-TADF nonacene for high-performance organic light-emitting diodes. Angew Chem Int Ed, 2023, 62: e202215522

[59] Park J, Kim SC, Jo U, *et al*. A design strategy for multiple resonance-induced pure violet thermally activated delayed fluorescence emitters with a narrow emission band. Adv Opt Mater, 2024, 12: 2301626

[60] Naveen KR, Oh JH, Lee HS, *et al*. Tailoring extremely narrow FWHM in hypsochromic and bathochromic shift of polycyclo-heteraborin MR-TADF materials for high-performance OLEDs. Angew Chem Int Ed, 2023,62: e202306768

[61] Meng G, Dai H, Zhou J, *et al*. Wide-range color-tunable polycyclo-heteraborin multi-resonance emitters containing B-N covalent bonds. Chem Sci, 2023,14: 979–986

[62] Hou P, Xu Y, Miao J, *et al*. Naphthalene-embedded multi-resonance emitters enabling efficient narrow emissive blue OLEDs. Chem Eur J, 2023,29: e202301931

[63] Jin J, Duan C, Jiang H, *et al*. Integrating asymmetric O-B-N unit in multi-resonance thermally activated delayed fluorescence emitters towards high-performance deep-blue organic light-emitting diodes. Angew Chem Int Ed, 2023, 62: e202218947

[64] Li G, Du M, Fan T, *et al*. Asymmetric structural design of a highly oriented multi-resonance emitter enables a

record 41.5% external quantum efficiency in deep-blue OLED. Mater Today, 2024, 73: 30–37

[65] Lee T, Jang J.-H, Nguyen NNT, *et al*. *Ortho*-carborane decorated multi-resonance TADF emitters: preserving local excited state and high efficiency in OLEDs. Adv Sci, 2024, 11: 2309016

[66] Hu J.-J, Wei Y, Wang X.-Z, *et al*. Efficient ultra-narrowband OLEDs based on carbazole-fused dual-boron embedded multi-resonance thermally activated delayed fluorescence materials. Adv Opt Mater, 2024, 12: 2302987

[67] Mamada M, Aoyama A, Uchida R, *et al*. Efficient deep-blue multiple-resonance emitters based on azepine-decorated *v*-DABNA for CIE_y below 0.06. Adv Mater, 2024, 36: 2402905

[68] Ye Z, Wu H, Xu Y, *et al*. Deep-blue narrowband hetero[*6*]helicenes showing circularly polarized thermally activated delayed fluorescence toward high-performance OLEDs. Adv Mater, 2024, 36: 2308314

[69] He X, Lou J, Li B, *et al*. Rational medium-range charge transfer strategy toward highly efficient violet-blue organic light-emitting diodes with narrowed emission. Adv Mater, 2024, 36: 2310417

[70] Ochi J, Yamasaki Y, Tanaka K, *et al*. Highly efficient multi-resonance thermally activated delayed fluorescence material toward a BT.2020 deep-blue emitter. Nat Commun, 2024, 15*:* 2361

[71] Weerasinghe RW, Suresh SM, Hall D, *et al*. A boron, nitrogen, and oxygen doped ***π***-extended helical pure blue multiresonant thermally activated delayed fluorescent emitter for organic light emitting diodes that shows fast k_{RISC} without the use of heavy atoms. Adv Mater, 2024, 36: 2402289

[72] Wan D, Zhou J, Yang Y, *et al*. Peripheral substitution engineering of MR-TADF emitters embedded with B–N covalent bond towards efficient BT.2020 blue electroluminescence. Adv Mater, 2024, 36: 2409706

[73] Cai X, Pan Y, Li C, *et al*. Nitrogen-embedding strategy for short-range charge transfer excited states and efficient narrowband deep-blue organic light-emitting diodes. Angew Chem Int Ed, 2024, 63: e202408522

[74] Wu L, Mu X, Liu D, *et al*. Regional functionalization molecular design strategy: a key to enhancing the efficiency of multi-resonance OLEDs. Angew Chem Int Ed, 2024, 63: e202409580 (2024)

[75] Song X.-F, Luo S, Li N, *et al*. Gold coordination-accelerated multi-resonance TADF emission for efficient solution-processible ultrapure deep-blue OLEDs. Angew Chem Int Ed, 2024, 63: e202413536

[76] Wang Y, Lv Z.-Y, Chen Z.-X, *et al*. Multiple-resonance thermally activated delayed fluorescence materials based on phosphorus central chirality for efficient circularly polarized electroluminescence. Mater Horiz, 2024,11: 4722–4729

[77] Jin J, Chen M, Jiang H, *et al*. Construction of hybrid long- and short-range charge transfer excitations for high-performance deep-blue electroluminescence with CIE_y < 0.04 and EQE > 35%. ACS Materials Lett, 2024,6: 3246−3253

[78] Hua T, Cao X, Miao J, *et al*. Deep-blue organic light-emitting diodes for ultrahigh-definition displays. Nat Photon, 2024,18: 1161–1169

[79] Lee KH, Lee JY. Phosphor sensitized thermally activated delayed fluorescence organic light-emitting diodes with ideal deep blue device performances. J Mater Chem C, 2019, 7: 8562−8568

[80] Zhang D, Song X, Gillett AJ, *et al*. Efficient and stable deep-blue fluorescent organic light emitting diodes employing a sensitizer with fast triplet upconversion. Adv Mater, 2020, 32: 1908355

[81] Nam S, Kim JW, Bae HJ, *et al*. Improved efficiency and lifetime of deep-blue hyperfluorescent organic light-emitting diode using Pt(II) complex as phosphorescent sensitizer. Adv Sci, 2021, 8: 2100586

[82] Lo K.-W, Tong GSM, Cheng G, *et al*. Dinuclear Pt^{II} complexes with strong blue phosphorescence for operationally stable organic light-emitting diodes with EQE up to 23 % at 1000 cd m^{-2}. Angew Chem Int Ed, 2022, 61: e202115515

[83] Wang Y, Di K, Duan Y, *et al*. The selective regulation of borylation site based on one-shot electrophilic C–H borylation reaction, achieving highly efficient narrowband organic light-emitting diodes. Chem Eng J, 2022, 431:133221

[84] Yang X, Zhou X, Zhang Y.-X, *et al*. Blue phosphorescence and hyperluminescence generated from imidazo[4,5-*b*]pyridin-2-ylidene-based iridium(III) phosphors. Adv Sci, 2022, 9: 2201150

[85] Qin Y, Yang X, Jin J, *et al*. Facially coordinated, tris-bidentate purin-8-ylidene Ir(III) complexes for blue electrophosphorescence and hyperluminescence. Adv Opt Mater, 2022, 10: 2201633

[86] Cheon H.-J, Woo S.-J, Baek S.-H, *et al*. Dense local triplet states and steric shielding of a multi-resonance TADF emitter enable high-performance deep-blue OLEDs. Adv Mater, 2022, 34: 2207416

[87] Lv X, Miao J, Liu M, *et al*. Extending the π-skeleton of multi-resonance TADF materials towards high-efficiency narrowband deep-blue emission. Angew Chem Int Ed, 2022, 61: e202201588

[88] Stavrou K, Suresh SM, Hall D, *et al*. Emission and absorption tuning in TADF B,N-doped heptacenes: toward ideal-blue hyperfluorescent OLEDs. Adv Opt Mater, 2022, 10: 2200688

[89] Kim E, Park J, Jun M, *et al*. Highly efficient and stable deep-blue organic light-emitting diode using phosphor-sensitized thermally activated delayed fluorescence. Sci Adv, 2022, 8: eabq1641

[90] Zhu Z.-L, Gnanasekaran P, Yan J, *et al*. Efficient blue electrophosphorescence and hyperphosphorescence generated by bis-tridentate iridium(III) complexes. Inorg Chem, 2022, 61: 8898−8908

[91] Fan T, Zhang Y, Wang L, *et al*. One-shot synthesis of B/N-doped calix[4]arene exhibiting narrowband multiple resonance fluorescence. Angew Chem Int Ed, 2022, 61: e202213585

[92] Mubarok H, Amin A, Lee T, *et al*. Triptycene-fused sterically shielded multi-resonance TADF emitter enables

high-efficiency deep blue OLEDs with reduced dexter energy transfer. Angew Chem Int Ed, 2023, 62: e202306879

[93] Yan J, Feng Z.-Q, Wu Y, *et al*. Blue electrophosphorescence from iridium(III) phosphors bearing asymmetric Di-*N*-aryl6-(trifluoromethyl)-2*H*-imidazo[4,5-*b*]pyridin-2-ylidene chelates. Adv Mater, 2024, 36: 2305273

[94] Yan J, Zhou D.-Y, Liao L.-S, *et al*. Electroluminescence and hyperphosphorescence from stable blue Ir(III) carbene complexes with suppressed efficiency roll-off. Nat Commun, 2023, 14: 6419

[95] Hou P, Xu Y, Miao J, *et al*. Naphthalene-embedded multi-resonance emitters enabling efficient narrow emissive blue OLEDs. Chem Eur J, 2023, 29: e202301931

[96] Wang S, Xu Y, Miao J, *et al*. Peripheral decoration of multi-resonance TADF emitter for narrowband blue OLEDs. Chem Eng J, 2023, 471: 144664

[97] Wang X, Wang L, Meng G, *et al*. Improving the stability and color purity of a BT.2020 blue multiresonance emitter by alleviating hydrogen repulsion. Sci Adv, 2023, 9: eadh1434

[98] Wu C, Tong K.-N, Shi K, *et al*. New [3+2+1] iridium complexes as effective phosphorescent sensitizers for efficient narrowband saturated-blue hyper-OLEDs. Adv Sci, 2023, 10: 2301112

[99] Huang T, Wang Q, Zhang H, *et al*. Enhancing the efficiency and stability of blue thermally activated delayed fluorescence emitters by perdeuteration. Nat Photon, 2024, 18: 516–523

[100] Cheong K, Han SW, Lee JY. Tetradentate Pt(II) complexes with bulky carbazole moieties for high-efficiency and narrow-emitting blue organic light-emitting devices. Small Methods, 2024, 8: 2301710

[101] Cheong K, Jo U, Hong WP, *et al*. Fused cycloalkyl unit-functionalized tetradentate Pt(II) complexes for efficient and narrow-emitting deep blue organic light-emitting diodes. Small Methods, 2024, 8: 2300862

[102] Yan J, Wu C, Tong K.-N, *et al*. Structural engineering of iridium(III) phosphors with imidazo[4,5-*b*]pyrazin-2-ylidene cyclometalates for efficient blue electroluminescence. Small Methods, 2024, 8: 2301555

[103] Yan J, Nakamura T, Tan X, *et al*. Blue electroluminescence from homoleptic Ir(III) carbene phosphors and peripheral decorated multiple resonance boron emitters. Chem Eng J, 2024, 488: 150791

[104] Zheng Z, Wang L, Xin Y, *et al*. Iridium(III) carbene phosphors with fast radiative transitions for blue organic light emitting diodes and hyperphosphorescence. Adv Funct Mater, 2024, 34: 2311692

[105] Wu Y, Xin Y, Pan Y, *et al*. Ir(III) metal emitters with cyano-modified imidazo[4,5-*b*]pyridin-2-ylidene chelates for deep-blue organic light-emitting diodes. Adv Sci, 2024, 11: 2309389

[106] Li G, Du M, Fan T, *et al*. Asymmetric structural design of a highly oriented multi-resonance emitter enables a record 41.5% external quantum efficiency in deep-blue OLED. Mater Today, 2024, 73: 30–37

[107] Yan J, Pan Y, Peng I.-C, *et al*. Selective syntheses of homoleptic Ir(III) complexes bearing di-CF_3-functionalized benzoimidazol-2-ylidenes for generation of blue phosphorescence. Inorg Chem Front, 2024, 11: 2413–2426

[108] Wang J, Zou P, Chen L, *et al.* Promising interlayer sensitization strategy for the construction of high-performance blue hyperfluorescence OLEDs. Light: Science & Applications, 2024,13: 139

[109] Xue Z, Chen G, Chen Z, *et al*. Planar expansion enhances horizontal orientation of multi-resonance TADF emitter toward highly efficient narrowband blue OLEDs. Adv Funct Mater, 2024, 34: 2409244

Cartesian coordinates of the optimized structures

PtODP_S_0

C	-0.92003800	3.16854100	2.91330900
C	-2.83773000	1.66177300	1.56729700
C	-0.65320700	1.81354200	2.64638000
C	-2.06718200	3.77258700	2.44162700
C	-3.08076200	3.08743400	1.66377600
C	-1.64820000	1.04712700	2.00410700
H	0.27588500	1.34768800	2.95738700
H	-2.21487000	4.83678900	2.61420800
H	-5.68878000	2.10961500	2.54573400
C	-5.98892400	1.20148200	2.03691700
C	-6.74197700	-1.17893200	0.63959700
C	-5.10380900	0.54255300	1.18448600
C	-7.26375000	0.65386800	2.17087500
C	-7.63153900	-0.51547400	1.48530500
C	-5.46460500	-0.63428400	0.49666300
H	-7.98555300	1.14067300	2.82001900
H	-8.63159400	-0.91856700	1.61614600
H	-7.04039800	-2.08840500	0.13426500
N	-3.76033300	0.81239800	0.86487100
C	-3.31525600	-0.12525600	0.00686500
N	-4.32014500	-1.02628400	-0.21896400
C	-3.88909100	-2.30016900	-0.70090800
C	-2.82891800	-4.73262900	-1.49758100
C	-2.47735100	-2.45170400	-0.70519800
C	-4.75148500	-3.30458600	-1.11771600
C	-4.19973000	-4.53326700	-1.51201200
C	-1.96964000	-3.68919000	-1.10016400
H	-5.82196100	-3.14909300	-1.16461200

H	-4.85727900	-5.33522600	-1.83441800
H	-2.39045100	-5.67977500	-1.79483000
O	-0.64806400	-4.02287700	-1.13477500
H	3.75570400	-3.81468600	-0.45570500
C	2.82455700	-3.26417800	-0.54152600
C	0.33640200	-1.80237500	-0.69249100
C	2.79872600	-1.87586500	-0.35710000
C	1.63509000	-3.91132100	-0.82604600
C	0.42150700	-3.19243500	-0.88138200
C	1.57677700	-1.18193800	-0.48184700
H	1.60184500	-4.98517500	-0.97767700
C	3.80315200	-0.91354500	0.01724100
C	5.20557100	1.38858500	0.92000300
C	5.14541000	-0.97639800	0.37853400
C	3.18554900	0.35742700	0.08700200
C	3.86457300	1.49601700	0.55906500
C	5.86069700	0.14938600	0.81795400
H	3.35089700	2.44230000	0.67922200
H	5.73270600	2.26126900	1.29377800
N	1.82502500	0.20698500	-0.27895600
C	1.02560700	1.24693700	-0.77585100
C	-0.54275700	3.34017100	-1.63202700
C	1.61686800	2.39583700	-1.32433900
N	-0.31844500	1.10833200	-0.74332400
C	-1.06865400	2.15088300	-1.15811500
C	0.84669200	3.47652800	-1.75641600
H	2.69241900	2.41735700	-1.42796900
H	-2.14006200	2.01426200	-1.09906900
H	-1.22958500	4.12784800	-1.91279000
C	1.52453900	4.72239800	-2.34583700
C	0.49935700	5.79602500	-2.75784700
H	1.02454000	6.66637000	-3.16625200
H	-0.09703600	6.14010000	-1.90542800
H	-0.18572700	5.43150100	-3.53157000
C	2.33948900	4.31541600	-3.59716200
H	2.82654700	5.19738500	-4.02935800
H	1.69197500	3.87479300	-4.36351800
H	3.12128700	3.58679300	-3.35842300
C	2.47432700	5.33292200	-1.28769200
H	2.95974800	6.22909900	-1.69152400
H	3.26294700	4.63185600	-0.99435900
H	1.92444000	5.62203600	-0.38498100
C	7.19796400	-0.33836100	1.10572000
C	9.44192400	-1.96881100	1.42708000

C	8.39211700	0.22714400	1.56848800
C	7.16632900	-1.71673200	0.81656700
C	8.26152400	-2.55512200	0.96371600
C	9.50592400	-0.59739800	1.72507700
H	8.45193500	1.28668700	1.80145100
H	8.19551300	-3.61244300	0.72966800
H	10.43966800	-0.17353800	2.08357000
H	10.32526500	-2.58708400	1.55875100
O	5.91985500	-2.11110300	0.37573200
Pt	-1.40697400	-0.79157900	-0.41775100
H	-0.19644100	3.76025600	3.46951700
C	-1.37823100	-0.37666800	1.84070500
H	-0.38994100	-0.70712600	2.15039400
C	-4.11885000	3.78350600	1.08597000
H	-4.86588300	3.30782600	0.46149500
H	-4.20359400	4.85568600	1.22919900
H	-2.16113000	-1.08079300	2.11279600

PtODP_T_1

C	-2.38853100	4.20508700	1.78888700
C	-3.16474800	1.62745000	1.08302200
C	-1.88076700	3.11248000	2.48483900
C	-3.28688100	4.00312600	0.74796600
C	-3.70722600	2.71868400	0.36601000
C	-2.25676300	1.80601700	2.15292700
H	-1.18637000	3.27415200	3.30391600
H	-3.68099000	4.86084900	0.20761000
H	-5.63884000	1.28556600	2.50873600
C	-5.72505500	0.27158200	2.13408200
C	-5.90002300	-2.41230600	1.18336700
C	-4.76185400	-0.26191700	1.27661600
C	-6.78686900	-0.55723700	2.50245900
C	-6.86883400	-1.87683300	2.03667800
C	-4.84309700	-1.58273300	0.79711100
H	-7.55386300	-0.17477200	3.16950200
H	-7.69698300	-2.50495400	2.35133300
H	-5.96308900	-3.44452100	0.86678700
N	-3.58228200	0.28584500	0.77033000
C	-2.88823700	-0.64497800	0.02365300
N	-3.69904900	-1.77079100	0.01868300
C	-3.17400200	-2.94159900	-0.57818700
C	-1.93121300	-5.14029500	-1.72149400
C	-1.79215600	-2.84295700	-0.85385200
C	-3.93949900	-4.06075000	-0.91470300

C	-3.30069900	-5.16404400	-1.49013400
C	-1.20137900	-3.98292400	-1.40220400
H	-5.01348000	-4.07128200	-0.77972700
H	-3.88037400	-6.04340800	-1.75464400
H	-1.40815100	-5.99148800	-2.14487600
O	0.14517000	-4.09774300	-1.65954800
H	4.48254300	-3.56556400	-0.81410400
C	3.50109600	-3.11151700	-0.88887800
C	0.85792800	-1.83555000	-0.98743500
C	3.31344900	-1.73469700	-0.53763100
C	2.40207600	-3.82100300	-1.30025800
C	1.11402900	-3.21919300	-1.31858100
C	2.02050300	-1.14556800	-0.66580900
H	2.47225400	-4.86915500	-1.57248800
C	4.17567200	-0.75930200	-0.00682400
C	5.28827300	1.56587400	1.22580700
C	5.51346900	-0.72421400	0.42362100
C	3.41777000	0.45636400	0.17642800
C	3.95894500	1.58687300	0.80378000
C	6.08048800	0.40207200	1.01939000
H	3.34767900	2.46354300	0.98494600
H	5.70906700	2.43191200	1.72659600
N	2.12303500	0.22819200	-0.30273500
C	1.25848900	1.22269800	-0.78913400
C	-0.42225100	3.15057500	-1.78173800
C	1.77878700	2.43425100	-1.25495100
N	-0.07502200	0.93456200	-0.85545100
C	-0.86763600	1.91551200	-1.36490800
C	0.95807400	3.44682700	-1.75618600
H	2.85395400	2.55697800	-1.25063500
H	-1.91410300	1.66055400	-1.42966100
H	-1.15294400	3.86252900	-2.14453100
C	1.56159400	4.75570600	-2.28136300
C	0.47272800	5.75449500	-2.71779500
H	0.93983800	6.68277100	-3.06544800
H	-0.19855200	6.01062200	-1.88985900
H	-0.13341600	5.36258500	-3.54232000
C	2.46485500	4.45230200	-3.50173800
H	2.91037500	5.37823800	-3.88603400
H	1.88784100	3.99045600	-4.31080000
H	3.28183200	3.77051800	-3.24236100
C	2.41023200	5.42005600	-1.17048000
H	2.84547900	6.35858600	-1.53491000
H	3.23594800	4.77731200	-0.84672900

H	1.79690300	5.64834400	-0.29116100
C	7.44585700	0.02851000	1.31946900
C	9.84305300	-1.39115600	1.56861100
C	8.55546200	0.65492000	1.90592500
C	7.58016400	-1.30403900	0.87451900
C	8.75161300	-2.03716100	0.98115000
C	9.74345200	-0.06449500	2.02363100
H	8.49223400	1.67971600	2.26108500
H	8.80924500	-3.06037600	0.62486000
H	10.61122000	0.40780200	2.47573100
H	10.78290100	-1.92514300	1.67453800
O	6.40029000	-1.76467800	0.32845100
Pt	-0.96034100	-1.04462500	-0.66104000
H	-2.08408800	5.21334700	2.05746600
C	-4.74466200	2.68782400	-0.77245000
H	-4.45301100	3.52559700	-1.42126800
C	-6.15332800	3.03069800	-0.23558200
H	-6.14571800	3.95424600	0.35326500
H	-6.54063900	2.22600300	0.39744400
H	-6.85090600	3.16499300	-1.07089400
C	-4.82472900	1.45415100	-1.68840100
H	-5.29497700	0.59804500	-1.19832000
H	-3.84821900	1.13447000	-2.06212800
H	-5.44350200	1.70843900	-2.55729000
C	-1.73089000	0.64110300	2.98924300
H	-1.99118600	-0.29050800	2.48143800
C	-0.19757700	0.65603300	3.12596500
H	0.13365000	-0.22904900	3.68109300
H	0.15953700	1.53765800	3.67176300
H	0.28567400	0.63776400	2.14470700
C	-2.40667300	0.62205900	4.37662500
H	-2.05233900	-0.23667400	4.95888600
H	-3.49617800	0.54617900	4.29158700
H	-2.17498300	1.53144600	4.94458800

PtON-TBBI_S_0

C	-0.38933200	-4.71714500	0.55640100
C	-3.18080000	-4.62201800	0.74948500
C	-1.12196100	-5.88965000	0.81293700
C	-1.02028100	-3.48341200	0.39128900
C	-2.43032200	-3.48511100	0.46514600
C	-2.50379700	-5.83567700	0.92053400
H	-0.58077500	-6.82303400	0.93288400
H	-5.24773800	1.38586200	-0.96348900

C	-5.33091200	0.32744500	-0.74384700
C	-5.51667000	-2.46822700	-0.22037200
C	-4.22036100	-0.41496000	-0.34764000
C	-6.54506700	-0.34789700	-0.86199200
C	-6.63178800	-1.72452700	-0.60641200
C	-4.29920600	-1.79417700	-0.08116800
H	-7.43211500	0.19916100	-1.16717200
H	-7.58631300	-2.23010700	-0.71942400
H	-5.60328900	-3.53445900	-0.06499800
N	-2.87365900	-0.05084300	-0.18349000
C	-2.12029200	-1.13865600	0.16996000
N	-3.00031200	-2.19192800	0.24792200
C	-2.37258300	1.24866400	-0.52428600
C	-1.49815400	3.75305500	-1.24808800
C	-1.41740800	1.37120100	-1.53266100
C	-2.89021700	2.36948900	0.12845800
C	-2.45994800	3.65242100	-0.23181400
C	-0.95630700	2.63944400	-1.90748900
H	-1.04781500	0.46901700	-2.00307800
H	-3.62050900	2.22143700	0.91496600
H	-1.15723800	4.74149600	-1.53986600
C	0.09225700	2.84027100	-3.01774400
C	1.30264100	3.61810200	-2.44779300
H	1.75526400	3.07628600	-1.60963700
H	1.01993400	4.61399700	-2.08950800
H	2.06750300	3.74909000	-3.22258500
C	-0.53828400	3.65124900	-4.17516800
H	-0.88801500	4.63476200	-3.84284800
H	-1.39419000	3.11914500	-4.60585000
H	0.19807400	3.81053400	-4.97216200
C	0.60591000	1.50352200	-3.58736400
H	1.07953600	0.88295700	-2.81883200
H	1.35532100	1.69902600	-4.36231100
H	-0.19819300	0.92021900	-4.05018800
C	-3.00260200	4.92741100	0.44235000
C	-3.69027800	5.81652200	-0.62172200
H	-4.53205400	5.29126600	-1.08739800
H	-2.99814700	6.10919100	-1.41819100
H	-4.07555600	6.73395900	-0.16040600
C	-1.83421700	5.71179900	1.08527200
H	-1.08697300	6.01193200	0.34359300
H	-1.32696800	5.10517100	1.84465200
H	-2.20743000	6.62171100	1.57054800
C	-4.03336500	4.61497400	1.54431300

H	-4.90857200	4.08723700	1.14842800
H	-4.38837700	5.54979000	1.99229400
H	-3.60257300	4.00746300	2.34862900
Pt	-0.13832100	-1.70194500	0.34702600
O	0.96119000	-4.92129100	0.48942400
C	1.90201800	-3.97147400	0.15741300
C	4.03446300	-2.38843500	-0.62499000
C	1.68117900	-2.58400400	0.17973900
C	3.12789000	-4.56202100	-0.21613300
C	4.19240700	-3.77884600	-0.62820700
C	2.81138600	-1.83934500	-0.18457400
H	3.19725600	-5.64508400	-0.20669200
H	5.12305300	-4.23624700	-0.95243700
N	2.92259400	-0.41261200	-0.23295800
C	4.17946600	-0.09716200	-0.80514800
C	4.88937900	-1.29866800	-1.04054000
C	5.96137300	1.16084700	-1.80300000
C	6.15512700	-1.25224100	-1.63474300
C	4.69795100	1.13643600	-1.20788000
C	6.69072100	-0.01985300	-2.00371400
H	4.13365700	2.05539400	-1.09288900
H	6.37660400	2.11266600	-2.12268500
C	2.19227500	0.45277300	0.58379600
C	0.76373500	2.14584200	2.21954100
N	0.87931600	0.19508600	0.79431000
C	2.82819400	1.53691900	1.21672500
C	2.13005900	2.41511500	2.04230800
C	0.20714100	1.03689900	1.60838900
H	3.89524200	1.64695800	1.08430200
H	-0.83249600	0.78557100	1.76874500
H	0.13167600	2.76540700	2.84270300
C	2.86255300	3.57262500	2.73773200
C	1.89906900	4.46544400	3.54294100
H	2.45885500	5.28437200	4.00785200
H	1.40146400	3.91112700	4.34661200
H	1.12832700	4.91251100	2.90424400
C	3.56774000	4.45075400	1.67698700
H	4.08527800	5.28544000	2.16429500
H	2.84550800	4.86829000	0.96601600
H	4.31392200	3.88694000	1.10746500
C	3.91857700	2.99058000	3.70858300
H	4.45355100	3.80374500	4.21350500
H	4.65843000	2.37639300	3.18516800
H	3.44625100	2.36630000	4.47533900

H	6.70668500	-2.17028500	-1.81899200
H	7.67246600	0.02591900	-2.46697200
H	-3.06663600	-6.73865900	1.13884700
H	-4.25406300	-4.58352600	0.87878800

PtON-TBBI_T_1

C	0.61460300	-4.69815700	0.50482600
C	-2.12153200	-5.19016600	0.70952100
C	0.16300800	-6.00880200	0.74221100
C	-0.25788800	-3.60366200	0.36716300
C	-1.65416200	-3.90392800	0.43337700
C	-1.20130800	-6.23671900	0.85830200
H	0.89004100	-6.80822300	0.83539100
H	-5.43304200	0.26548500	-0.90849100
C	-5.28662700	-0.78381200	-0.67987000
C	-4.87861500	-3.54954000	-0.13934100
C	-4.03116900	-1.27059200	-0.31170300
C	-6.33958800	-1.69809200	-0.76143400
C	-6.13884300	-3.05747800	-0.49637100
C	-3.82168700	-2.64105300	-0.04238600
H	-7.32767700	-1.34522800	-1.04289400
H	-6.97167700	-3.75008100	-0.57448400
H	-4.74245600	-4.60905300	0.02621200
N	-2.79700200	-0.62834400	-0.19133800
C	-1.80536900	-1.53822400	0.16469400
N	-2.45937500	-2.77466700	0.23698700
C	-2.58910400	0.73528000	-0.55404500
C	-2.24778100	3.37081000	-1.29597800
C	-1.65930200	1.05564200	-1.54532800
C	-3.33922200	1.73396000	0.07597500
C	-3.18494000	3.07543700	-0.29581000
C	-1.46879500	2.38780000	-1.92764400
H	-1.09806500	0.24947700	-1.99992000
H	-4.03337200	1.44502500	0.85594500
H	-2.11701300	4.40652900	-1.59383300
C	-0.45496500	2.79408100	-3.01479400
C	0.55862000	3.80075100	-2.41953700
H	1.08676100	3.36220200	-1.56517800
H	0.06983900	4.71841100	-2.07484400
H	1.30176400	4.08299300	-3.17533900
C	-1.20286400	3.45968500	-4.19481400
H	-1.75479000	4.35112300	-3.87765500
H	-1.92030900	2.76447000	-4.64552900
H	-0.49190300	3.76550700	-4.97221800

C	0.33135700	1.58672500	-3.55997900
H	0.89359700	1.07413500	-2.77166700
H	1.05018200	1.92577400	-4.31458300
H	-0.32733900	0.85406100	-4.03988300
C	-3.99560700	4.21217800	0.35714200
C	-4.82402100	4.94149400	-0.72754600
H	-5.52739400	4.25369600	-1.21080300
H	-4.18736900	5.37052400	-1.50829900
H	-5.40156000	5.76003100	-0.28058800
C	-3.02953300	5.21878700	1.02633500
H	-2.33228300	5.65800300	0.30519600
H	-2.43683400	4.72947400	1.80831100
H	-3.59225700	6.03885000	1.48887100
C	-4.96873200	3.69614600	1.43447100
H	-5.70528500	2.99821100	1.02011300
H	-5.52070700	4.53828200	1.86659300
H	-4.44273700	3.19209200	2.25334700
Pt	0.23882700	-1.69436000	0.34101200
O	1.97165000	-4.60022900	0.40207100
C	2.71045600	-3.49220700	0.14504100
C	4.45467900	-1.48938900	-0.60072500
C	2.18870300	-2.16858800	0.19005700
C	4.04647800	-3.81918200	-0.21752600
C	4.91487000	-2.83362800	-0.61836400
C	3.14727600	-1.20459700	-0.14850900
H	4.33263200	-4.86578800	-0.21646600
H	5.92070300	-3.07284700	-0.94874400
N	2.94653300	0.20090500	-0.20392700
C	4.09134900	0.77054300	-0.78031800
C	5.05014100	-0.25581500	-1.01608400
C	5.56955300	2.37460400	-1.77063100
C	6.28376400	0.05974700	-1.61228900
C	4.34215200	2.08929100	-1.17674200
C	6.54048400	1.37328300	-1.97634500
H	3.59843900	2.86815600	-1.05344700
H	5.77576500	3.39205700	-2.09096600
C	2.03259300	0.89346300	0.62156300
C	0.24655400	2.24111500	2.21019400
N	0.79595600	0.34750300	0.79598900
C	2.42248300	2.06280500	1.27246600
C	1.53599900	2.78848900	2.08566100
C	-0.06133600	1.04617100	1.59266900
H	3.44679900	2.39137300	1.15885700
H	-1.03132000	0.58822000	1.72933800

H	-0.52073400	2.71736000	2.80806000
C	1.99583200	4.06826400	2.79353300
C	0.86876100	4.69509300	3.63610700
H	1.23428400	5.60616800	4.12285400
H	0.52303700	4.01572900	4.42358300
H	0.00595000	4.97335900	3.01973200
C	2.44879700	5.10631900	1.73794400
H	2.77831000	6.03029700	2.22880000
H	1.62778100	5.35660100	1.05637800
H	3.28506200	4.73472900	1.13566300
C	3.18335000	3.74449800	3.73264600
H	3.52450800	4.65463000	4.24122900
H	4.03597800	3.33084000	3.18379100
H	2.89138600	3.01554600	4.49681200
H	7.01855500	-0.71976700	-1.79407100
H	7.48808400	1.63310800	-2.43928100
H	-1.56552900	-7.23888600	1.06464500
H	-3.17548700	-5.39154800	0.84325400